REPORT DOCUMENTATION PAGE

Form Approved OMB NO. 0704-0188

1. REPORT DATE (DD-MM-YYYY)	2. REPORT TYPE	3. DATES COVERED (From - To)
25-04-2012	Final Report	30-Jun-2010 - 29-Jun-2011

4. TITLE AND SUBTITLE
A Hardware Testbed for Distributed Learning, Estimation, and Approximation Theory with Sensor Vehicle Networks

5a. CONTRACT NUMBER
W911NF-10-1-0283

5b. GRANT NUMBER

5c. PROGRAM ELEMENT NUMBER
611103

6. AUTHORS
A. Kurdila, A. Leonessa

5d. PROJECT NUMBER

5e. TASK NUMBER

5f. WORK UNIT NUMBER

7. PERFORMING ORGANIZATION NAMES AND ADDRESSES
Virginia Polytechnic Institute & State University
Office of Sponsored Programs
Virginia Polytechnic Institute and State University
Blacksburg, VA 24060 -

8. PERFORMING ORGANIZATION REPORT NUMBER

9. SPONSORING/MONITORING AGENCY NAME(S) AND ADDRESS(ES)
U.S. Army Research Office
P.O. Box 12211
Research Triangle Park, NC 27709-2211

10. SPONSOR/MONITOR'S ACRONYM(S)
ARO

11. SPONSOR/MONITOR'S REPORT NUMBER(S)
57679-MA-RIP.1

12. DISTRIBUTION AVAILIBILITY STATEMENT
Approved for Public Release; Distribution Unlimited

13. SUPPLEMENTARY NOTES
The views, opinions and/or findings contained in this report are those of the author(s) and should not contrued as an official Department of the Army position, policy or decision, unless so designated by other documentation.

14. ABSTRACT
This report summarizes the design process and implementation of a hardware testbed for a distributed sensing network consisting of autonomous ground vehicles. The goal of the designed testbed is to support research in the synthesis of approximation, learning and estimation theory for high-bandwidth distributed sensing vehicle networks. The report describes the autonomous vehicle designed as the sensing node of the network, and the sensors configured for each node. Performance of sensing subsystems is described.

15. SUBJECT TERMS
distributed sensing, autonomous systems

16. SECURITY CLASSIFICATION OF:			17. LIMITATION OF ABSTRACT	15. NUMBER OF PAGES	19a. NAME OF RESPONSIBLE PERSON
a. REPORT	b. ABSTRACT	c. THIS PAGE			Andrew Kurdila
UU	UU	UU	UU		19b. TELEPHONE NUMBER: 540-231-8028

Report Title

A Hardware Testbed for Distributed Learning, Estimation, and Approximation Theory with Sensor Vehicle Networks

ABSTRACT

This report summarizes the design process and implementation of a hardware testbed for a distributed sensing network consisting of autonomous ground vehicles. The goal of the designed testbed is to support research in the synthesis of approximation, learning and estimation theory for high-bandwidth distributed sensing vehicle networks. The report describes the autonomous vehicle designed as the sensing node of the network, and the sensors configured for each node. Performance of sensing subsystems is described.

Enter List of papers submitted or published that acknowledge ARO support from the start of the project to the date of this printing. List the papers, including journal references, in the following categories:

(a) Papers published in peer-reviewed journals (N/A for none)

Received Paper

TOTAL:

Number of Papers published in peer-reviewed journals:

(b) Papers published in non-peer-reviewed journals (N/A for none)

Received Paper

TOTAL:

Number of Papers published in non peer-reviewed journals:

(c) Presentations

Number of Presentations: 0.00

Non Peer-Reviewed Conference Proceeding publications (other than abstracts):

Received Paper

TOTAL:

Number of Non Peer-Reviewed Conference Proceeding publications (other than abstracts):

Peer-Reviewed Conference Proceeding publications (other than abstracts):

Received Paper

TOTAL:

Number of Peer-Reviewed Conference Proceeding publications (other than abstracts):

(d) Manuscripts

Received	Paper

TOTAL:

Number of Manuscripts:

Books

Received	Paper

TOTAL:

Patents Submitted

Patents Awarded

Awards

None during the reporting period

Graduate Students

NAME	PERCENT_SUPPORTED

FTE Equivalent:

Total Number:

Names of Post Doctorates

NAME	PERCENT_SUPPORTED

FTE Equivalent:

Total Number:

Names of Faculty Supported

NAME	PERCENT_SUPPORTED

FTE Equivalent:

Total Number:

Names of Under Graduate students supported

NAME	PERCENT SUPPORTED

FTE Equivalent:

Total Number:

Student Metrics

This section only applies to graduating undergraduates supported by this agreement in this reporting period

The number of undergraduates funded by this agreement who graduated during this period:	0.00
The number of undergraduates funded by this agreement who graduated during this period with a degree in science, mathematics, engineering, or technology fields:.....	8.00
The number of undergraduates funded by your agreement who graduated during this period and will continue to pursue a graduate or Ph.D. degree in science, mathematics, engineering, or technology fields:.....	2.00
Number of graduating undergraduates who achieved a 3.5 GPA to 4.0 (4.0 max scale):	4.00
Number of graduating undergraduates funded by a DoD funded Center of Excellence grant for Education, Research and Engineering:	0.00
The number of undergraduates funded by your agreement who graduated during this period and intend to work for the Department of Defense	0.00
The number of undergraduates funded by your agreement who graduated during this period and will receive scholarships or fellowships for further studies in science, mathematics, engineering or technology fields:	0.00

Names of Personnel receiving masters degrees

NAME

Total Number:

Names of personnel receiving PHDs

NAME

Total Number:

Names of other research staff

NAME	PERCENT SUPPORTED

FTE Equivalent:

Total Number:

Sub Contractors (DD882)

Inventions (DD882)

Scientific Progress

See the attachment.

Technology Transfer

A Hardware Testbed for Distributed Learning, Estimation, and Approximation Theory with Sensor Vehicle Networks

A. Kurdila

A. Leonessa

Summary

This document summarizes the research efforts under the Army Research Office sponsored DURIP entitled "A Hardware Testbed for Distributed Learning, Estimation, and Approximation Theory with Sensor Vehicle Networks" (W911NF-10-1-0283, 57679-MA-RIP). The goal of this project has been to develop an autonomous mobile platform and sensing network suited to conducting research in 3D mapping and distributed approximationg from network sensing. Specifically, this document summarizes the efforts by the investigators to develop a team of robotic vehicles capable of off-road travel, waypoint navigation, and obstacle avoidance that will provide a robust platform for carrying 3D mapping hardware, onboard processing and telemetry. The system will take advantage of wavelet compression and/or compressive sensing techniques to make full use of limited bandwidth. Each of the individual vehicles in the sensor network are referred to as an Mapping Autonomous Ground Vehicle (MAGV) in this report.

In order to begin the process of creating the ideal platform for this project, a baseline of performance and design criteria was defined. These originated both from the project sponsor and project managers. Additionally, we used specifications from the International Ground Vehicle Competition (IGVC) as a source of specifications for our design, and restrictions present in the International IGVC rules were taken in to account. Once minimum requirements were established, these specifications translated to specific hardware limitations.

At the initiation of the effort, an extensive market and literature survey helped determine what types of platforms were commercially available. The research team decided that the available market platforms did not meet the needs of the project, and the platforms had to be designed and fabricated by the team. The team decomposed the platform design into two functional needs: the frame and the drivetrain. The design team formed two primary working groups to tackle these two tasks: the mechanical design and drivetrain design teams. The teams focused on the two individual design tasks while maintaining communication to ensure successful integration into a functional system.

The mechanical design team developed a frame capable of supporting the loads of the vehicle and providing structure for the individual components. The performance of the frame design was verified prior to fabrication using finite element analysis. The material was selected using a structured decision process and priced through a common supplier. The stock was then CNC machined and cut to length before being sent to a professional fabrication company for welding.

The drivetrain design team selected drivetrain components capable of powering and propelling the vehicle according to customer needs. These components include the batteries, motors, gearbox, and controller. The components were selected utilizing a structured decision

process and the costs were analyzed to ensure cost efficiency. The mechanical linkage of the drivetrain was also designed based on the CAD models provided by the motor supplier and in house drawings of our platform. When the frame fabrication had been completed, the drivetrain was assembled into the base.

Various sensing technologies were evaluated for use on each of the MAGV to demonstrate the effectiveness of high bandwidth 3D sensing for both archival and compressive sensing purposes. A visual spectrum camera, IR camera, 3D Time-of-Flight camera (Flash LiDAR), and GPS/INS were purchased and integrated into a LabVIEW operating environment. Additionally, a mechanical platform which can hold and rotate the visual spectrum camera as well as a flash LiDAR in tandem was designed and built. Finally, a compact multiple-beam rotating LIDAR system was acquired to capture very large 3D point clouds at long range outdoors.

After the sensing and autonomy capabilities were integrated into the MAGV platform, one of the prototype sensing vehicles was formally tested at the IGVC competition at Oakland University in Rochester, Michigan in June of 2011. The competition involved autonomous path following, obstacle avoidance, and waypoint navigation on a mild off-road terrain consisting of smooth and rutted grassy fields. This proving ground gave us valuable insight to the performance of our design, and allowed us to evaluate several of our previous design decisions, and incorporate our findings in to the construction of a next-generation platform.

In particular, it was found that on soft grass and ground, the vehicle had difficulty accelerating or turning in place after coming to a full stop. The caster wheels that allow the differential steering capability could become stuck, and the power of the drive motors was occasionally insufficient to overcome the initial resistance to get the vehicle moving. Secondly, the lack of a ride suspension on the vehicle caused excessive vibration that eventually lead to a minor structural failure due to material fatigue, despite the fact that the vehicle was driven only on grass and dirt. The limited damping provided by the pneumatic tires of the MAGV was not adequate for high-speed off road operation.

After the IGVC, a second generation design incorporating our findings was created and designated the Mark II. The MkII incorporated independent trailing swingarm suspension for both the drive wheels and the front casters, and drive motors with an increased power rating. Ride height was maintained using coilover spring-damper struts. The MkII was prototyped prior to formal fabrication, and it was found that the suspension design was unstable and not feasible.

The MkIII was then designed with a high strength independent parallel link suspension in the rear, and an air-spring trailing arm configuration in the front. The diameter of the drive wheels and the under-chassis ground clearance was increased to improve off road performance. The overall wheelbase was narrowed to improve maneuvering ability in close quarters. The

viability of the MkIII design was verified by constructing a single platform before fabrication of the remaining three vehicles in the fleet was started.

The MkIII is now being used in calibration and testing in data collection and sensor shakedown tests. The performance of the sensor node vehicle will be further evaluated at the June 2012 IGVC. In the meantime, the fleet of four MkIII ground vehicles will be used for independent and cooperative autonomous sensing research.

Table of Contents

Summary ……...……2

Introduction ……..…4

Mission and Objectives ……...4

Scope and Assumptions ……..……5

Approach and Methods Used in the Design Process……...……6

Design Process and Planning……...……6

Identification of Customer Needs……7

Conversion of Customer Needs to Engineering Performance Metrics……...…….8

Product Concept Generation……8

Concept Selection Result and Discussion…….....……10

Final Product Selection Analysis……...……..10

Final Product Specifications…….…13

3-D CAD Model……...……..13

Engineering Analysis……..…….....14

Material Selection……..……16

Drivetrain Design Results……..20

Sensor Selection…….31

Cost Analysis…….49

Ethical Considerations……...52

Performance Testing……..……...53

Design Evolution……..…….....53

Summary and Conclusions……56

References…….…….56

Appendix A: Customer Needs and House of Quality……...….57

Introduction

The Army requires a platform for future research efforts involving highg bandwidth sensor technologies. The need is for an autonomous ground vehicle network capable of carrying 3D mapping sensor technologies. The platform developed under this initiative will support research efforts involving 3D distributed sensing. There is currently a limited market of unmanned ground vehicle platforms to support research efforts. This project will overcome the market limitations by creating a design and platform to support continued sensor development and autonomy research.

The platform that constitutes the foundation of the sensor network will be a crucial tool in the continuing research in sensor technologies and autonomous vehicles. The system will offer a highly functional and robust network sensor testbed. It will provide a complete autonomous vehicle solution to support sensor package research for 3D mapping and future efforts in autonomous vehicle research. The benefits to the autonomous vehicle community and the broader engineering community will expand research capabilities and enhance the implementation of prototype sensing and autonomy systems.

Mission and Objectives

The mission goal was to design and implement the hardware and software necessary to provide an autonomous unmanned ground vehicle network capable of supporting efforts in sensor research and 3D mapping via distributed sensing. The research team has identified three functionally-based objectives to complete the mission goal: the complete integrated hardware of a vehicle platform, the complete hardware package necessary to realize a 3D sensor module, and control and autonomy capabilities. To achieve the functional objectives, the team pursued three tasks as follows: hardware design and implementation of the sensor node vehicle, software design and implementation, and autonomous operations capabilities. All of these tasks are interdependent and were performed in parallel. Completion of these tasks ultimately lead to accomplishing the functional objectives and the overall mission goal of an autonomous unmanned ground vehicle network platform for 3D mapping and distributed sensing.

Scope and Assumptions

The autonomous sensor network is being designed for research into distributed sensing with high bandwidth sensors including three dimensional LIDAR. The proposed vehicle must be able to complete basic obstacle avoidance, waypoint navigation, and data collection used for mapping. As such the design of a fully functioning vehicle requires focus in three general areas: design of the mechanical platform, the design of the three dimensional LIDAR, and integration of the required mapping sensors with control software to achieve complete autonomy. This project does not specifically deal with compressed sensing, simply the design of a professional

grade platform capable of collecting and processing the data required for future studies in the field. This platform is planned to used over the next five to ten years for a variety of applications. Any design should be easily modifiable for future applications and have sufficient room and computing power to accommodate additional sensors and payloads.

As a secondary objective, this robotics platform was also being designed to enter in the International Ground Vehicle Competition (IGVC) in June of 2011. The requirements of the competition provided a good mechanism for defining realistic performance criteria for the system. Moreover, the IGVC is a well-known forum that will provide a good venue for communicating the research carried out under the DURIP program to the robotics community. Entering this competition places a number of constraints on the design, particularly size and safety restrictions. IGVC rules require a minimum ground footprint of three feet in length and two feet in width. IGVC also requires the robot be equipped with both a wireless and hardwired emergency stop. IGVC requires the robot be capable of autonomous waypoint navigation, obstacle avoidance, and path following. Waypoint navigation and obstacle avoidance mesh well with the requirements of the military grant, but path following may require additional vision based sensing capabilities and will demand additional control programming.

Because this vehicle will likely be used for indoor as well as outdoor applications at some point in its lifespan, it must be rugged enough for a variety of environmental conditions without becoming too bulky for indoor navigation. Indoor navigation demands the robotic sensors must be able to fit through standard 30 inch door frame as well as navigate sharp corners and tight spaces, limiting the maximum size of the vehicle and implying a small turn radius. Outdoor use will require at least a minimal resistance to environmental factors, including light rain, dirt, grass, and sun exposure. In order to call the vehicle fully autonomous, it must be able to operate without interaction from an off-robot base station. Because the project is funded by the DoD, the design needs to have a professional appearance and robust construction.

Approach and Methods Used in the Design Process

This section defines the overall design process used, outlines the process used to identify DoD needs, converts those needs to measureable performance metrics, and employs the resulting metrics to develop design concepts.

Design Process and Planning. To solve the problem outlined in the mission statement, a variety of design methods and tools were employed to facilitate the research. Figure 1 shows a work breakdown used to assign tasks. This is a very broad outline that captures the process that has been used.

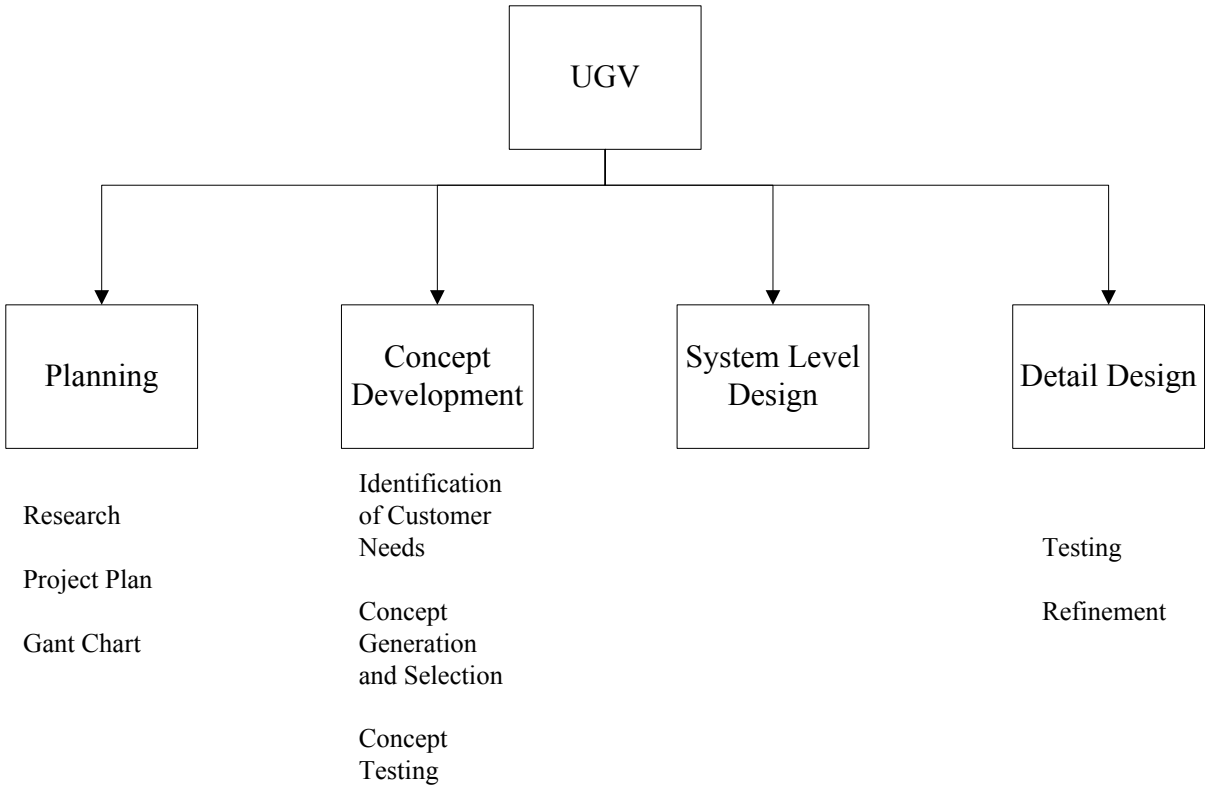

Figure 1. Work breakdown structure for the development of an autonomous unmanned ground vehicle research platform.

First, the planning stage developed a Gantt chart to establish goals and deadlines. Research in existing technologies helped us understand the problem and find viable solutions. The design process began with a review of the basics of robotics for the undergraduate and graduate researchers, and the investigators summarized how different sensors could be used to attain autonomy.

Identification of Customer Needs. After project planning, the design team began concept development. Since the design team was comprised of two investigators (Professors Kurdila and Leonessa) and 8 undergraduate students and two graduate students, the team was organized consistent with the principles of design taught in the undergraduate design in the Department of ME at VT. As such, the goals of the development in the project were cast in the form of deliverables to customers. The research sensing network to be developed by the team constituted the product of the design team. The DoD needs for the UGV were identified by examining the team's two primary customers. These two customers are the Army and the IGVC. The criteria for these two primary customers are shown in Table 1.

Table 1. Criteria established by the Army and the IGVC

	ARMY	IGVC
Operation Speed	0-10 mph	< 5 mpg
Battery Duration	8 hours	-
Maximum Size	-	7' x 5' x 6'
Minimum Size	3' x 2' x 1'	3' x 2' x -'
Maximum Mass	100 kg	-
Minimum Payload	20 kg	9 kg
Maximum Turning Radius	0 m	-
Mobility Goals	Paved roads, 4" curbs, rolling grassland	Rolling grassland
Autonomy Goals	Waypoint navigation, simple obstacle avoidance	Waypoint navigation, simple obstacle avoidance, emergency shutdown
Propulsion	Battery	Battery
Cost	$150,000	-

One can see there are quite a few differences between the specifications of the two customers. The goal has been to satisfy both customers. In general, the goals from the Army are much higher than those of the IGVC. It is important to note, however, that IGVC specifications are non-negotiable. Therefore, the IGVC specifications must be met, regardless of setbacks. The target specifications for the product are the goals established by the Army.

Conversion of Customer Needs to Engineering Performance Metrics. To build a product that met the customer needs, a set of engineering performance measures were established. These allowed the team to quantitatively rate and compare the performance of concept designs and existing products. A house of quality was built to do carry out this evaluation. It can be found in Appendix A. The house of quality compares each customer to each performance measure and rates the correlation.

Product Concept Generation. In the first stage of the design process a market research was conducted on existing platform. According to the technical specification given by the team's investigators, the selection of the platforms was limited by the top speed, dimensions, total weight, payload, turning radius, ground clearance, battery life, position accuracy and autonomy ability.

Among the above criteria, position accuracy and autonomy ability can be improved by using better sensors and implementing better controller programs. Therefore, the focus of the team has been on the hardware selection for the platform during the initial market research.

For each of the technical specifications, there are various realizations in the researched platforms. For example, as far as steering is concerned, traditional Ackermann steering, differential wheel/tread steering, skid steering, and four wheel Ackermann steering have been found to be popular on academic, military and commercial platforms.

DC motors, high speed servos, diesel engines and hybrid systems are the most common ways to drive a UGV or robot based on their size and application.

Many of the platforms embed the feature of waypoint navigation into their controller by using GPS with or without differential correction. However, since most are military vehicles, there is no access for the general public. In any case, most military vehicles are oversized for this project.

Research showed that among all the specifications desired, the balance between speed, turning radius and size/weight is the limiting factor in the selection of the platform. Most platforms under the size requirements cannot output a top speed at 10 mph, and zero radius turning vehicles tend to have a lower speed than Ackermann steering vehicles. Based on the balance among these specifications, the team narrowed down the collection of available platforms to three candidates. These will be discussed in more detail shortly. In summary, none of the available platforms met the criteria defined for the Army.

Concept Selection Result and Discussion

This section defines the final product selection, the specifications identified for the final product, 3-D CAD models of the design, and a brief cost analysis.

Final Product Selection Analysis. An extensive market survey was pared down to three models, on the basis that these came the closest to fitting all of the design requirements with little or no modification. Then, a more detailed product comparison was completed to determine the optimal platform for project needs. Upon a detailed analysis, the design team identified no platform which met the customer needs in a financially reasonable manner. Therefore, the team designed and priced a novel vehicle sensor node that met the needs of the customers.

The selection process began with a detailed analysis of the available platforms on the market. After extensive research, the team identified the Clearpath Robotics 'Husky A100', the ReflexRobotics 'Archer E' and the 21st Century Scientific 'Bounder' platforms.

Clearpath Robotics 'Husky A100'. The Husky A100 is a robotics research platform designed for light-duty off-road applications. Approximately three feet square, and two feet high, it has a differentially steered all time 6-wheel drivetrain. Capable of carrying a 45 kg payload, the platform is set up with large internal expandability. The Husky A100 has a top speed of 3 mph, and endurance of 2 hours, and so would require drivetrain and power system modification to meet these mobility requirements. See Figure 2 below for the Husky A100 [1].

Figure 2. Photograph of the Husky A100 robotics research platform manufactured by Clearpath Robotics [1].

ReflexRobotics 'Archer E'. The Archer is a robotics development platform designed for heavy off road use. With the suspension geometry and drivetrain of a commercial ATV, the Archer is capable of negotiating rough terrain, and reaching of top speed of 20 mph. The E variant, with its fully electric drive system, takes advantage of advanced features such as regenerative braking to achieve operational endurance of 8+ hours. At low speeds, the Archer takes advantage of front and rear wheel steering for a tight turning radius, but cannot achieve the zero-radius goal identified as an ideal mobility requirement. Figure 3 below shows the Archer E platform [2].

Figure 3. Photograph of the Archer E robotics development platform manufactured by Reflexx Robotics [2].

21st Century Scientific 'Bounder'. The Bounder is an electric wheelchair platform, designed for high speed operation. While the majority of wheelchairs have a top speed of 5 mph or less, the Bounder can reach 11.6 mph and has a high strength, rugged design. Differential steering with dual casters allows zero turning radius, and high capacity batteries give an endurance of 8+ hours. The Bounder is very customizable, and can be ordered with many different options in terms of frame dimension, drivetrain ratios, suspension, and ground clearance. See Figure 4 for the base mechanical platform of the Bounder [3].

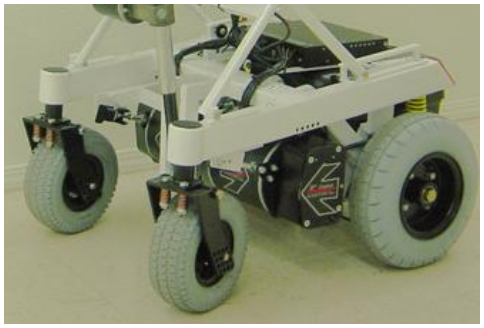

Figure 4. Photograph of the base mechanical platform for the Bounder electric wheelchair manufactured by 21st Century Scientific [3].

Below, Table 2 compares and contrasts the three platforms outlined above, and demonstrates the final design selection. Based on the market research and the comparison in Table 2 the Bounder electric wheelchair platform was selected as the most ideal candidate.

Table 2. Comparison of the three final mechanical platforms selected as possible platform options. The comparison shows the best option, based on measurable specifications, is the Bounder platform.

Design Requirement:	Husky A100	Archer E	Bounder
Payload: 40 kg	45 kg	90 kg	100+ kg
Speed: 10 mph	3 mph	20 mph	11.6 mph
Zero turning radius	Yes (differential skid)	No (low radius)	Yes (differential + caster)
Endurance: 8 hr	2 hr	8 hr	8+ hr
Affordability	$13,000	$17,000	$12,000

Meets or exceeds specification

Possible to meet specification with platform modification

Does not meet specification and cannot be modified to do so

The team requested a quote from 21st Century Scientific for the Bounder platform, with the configuration options that have been described. A brief outline of the quote can be found in Table 3. Based on the quote, the base mechanical platform will cost in excess of $13,800. As a complete wheelchair system, this price is reasonable due to the significant engineering effort to provide a cohesive and effective wheelchair system. However, as a decomposed mechanical system, the design team decided that the cost was far too high and an inefficient use of funds. With this in mind, the design team identified that the market could not supply the necessary mechanical platform. It was deemed necessary that a new vehicle sensor node must be designed and fabricated to meet the needs of the customers in a financially responsible manner.

Table 3. Brief outline of the selected Bounder platform cost based on a quote provided by the vendor, 21st Century Scientific [4].

Base Price	$ 10,345
Wide, Long Wheelbase	920
Extra Ground Clearance	460
Gel Cell Batteries	970
Drive Programmer	575
subtotal	$ 13,277
Shipping + Handling	550
Total	**$ 13,827**

To carry out the development in the project, the investigators created two primary working groups based on functional needs. The two teams for the development of the mechanical platform included the mechanical design team and the drivetrain design team. The mechanical design team was responsible for design and analysis of the frame and support structures. The drivetrain design team was responsible for battery, motor and gearbox selection. The teams worked closely to ensure that the result of both efforts integrated seamlessly into a functional system.

Mechanical Design Results. The mechanical design team pursued a frame structure to provide the underlying support for the entire vehicle. The goal was to produce a frame that supported the necessary components of a functional system. Specifically, the frame provides structure for the wheelbase and mounting locations for the drive wheels. Additionally, the primary supported load is the mass of the batteries. The team analyzed the three identified platforms above, and pursued a similar design that was customized specifically to the needs of the project.

Final product specifications and 3-D models. The following section outlines the results of the design process, including detailed specifications and expected performance.

In order to meet footprint requirements for the IGVC competition, a 36” length was selected, as measured from front to rear axles. Because it was felt that the robot should be able to pass through standard interior door frames, a width of 30” as measured from the limits of the drive tires was also selected.

Pneumatic tires with a 14” inflated height have been selected as optimal for the design. The flexible sidewalls provide a limited suspension for the vehicle, while the large diameter relative to the height of obstacles that must be traversed results in a large mechanical advantage, reducing the amount of power required to cross low bumps and curbs.

The ground clearance was another area of concern for the design of the frame. The position of the motor mounting points and selection of 14” tall tires result in a 5” ground clearance. According to the customer needs, this is more than adequate for all movement profiles and required terrain types.

The design team created a detail CAD model that has been iteratively updated in accordance with the needs of the design and the drivetrain team. An isometric 3-D model can be found in Figure 5.

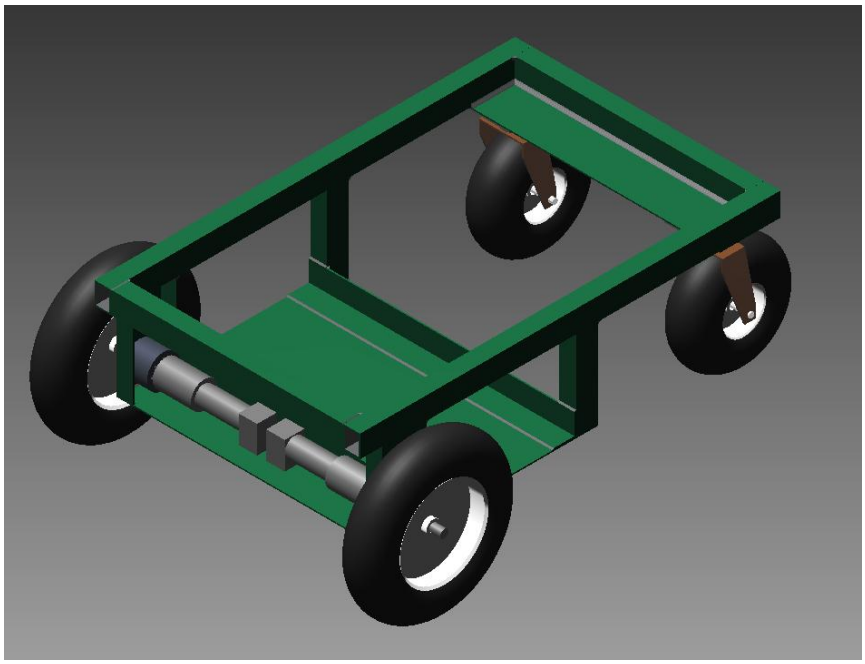

Figure 5. 3-D CAD image of the base mechanical platform that has been designed to meet all project requirements, with final specifications found in [4].

Engineering analysis. Based on the CAD models developed for the frame, the design team performed a basic finite element analysis of the frame structure. The finite element analysis revealed stress concentrations and areas of concern. The process began by defining the system constraints and loads. Then, the analysis was performed using the integrated finite element analysis software in Autodesk Inventor.

To begin, consider the constraints necessary to restrain the frame. The constraints as defined by the design are selected to be the four wheel locations. Therefore, the frame was constrained in the vertical direction at the four wheel mount locations: two casters near the rear of the frame and two drive wheels at the front of the frame. Next, the team identified the dominant static loads. In the case of the robot design, the primary mass of the vehicle is due to the batteries. Therefore, the dominant load was represented as an evenly distributed pressure load

that represents the weight of the batteries in their installed location. See Figure 6 below for a screenshot of the meshed frame with the applied pressure load.

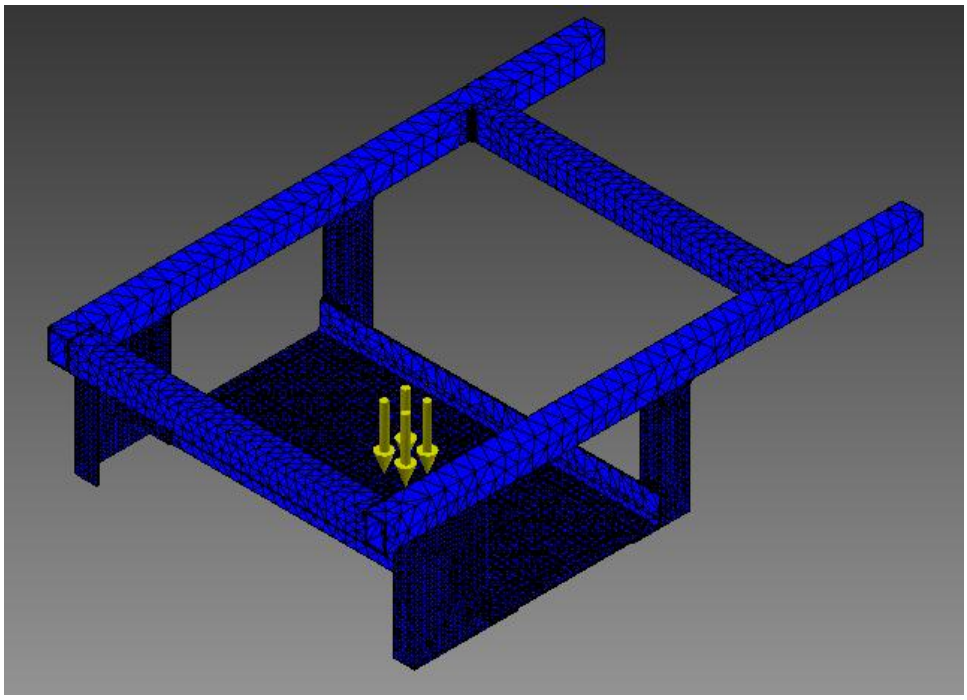

Figure 6. The image shows the constraints and loads applied to the frame for the finite element analysis. The constraints model the four wheels that limit vertical displacement. The load represents the weight of the batteries, the dominant force expected for static loading.

After applying the constraints and loads, the software was configured to ensure proper mesh density and stress convergence. In particular, the program was set to achieve convergence of the Von Mises stresses to within 2% of the true value. The resulting mesh contained about 128,000 elements with a predicted convergence of less than 1.1%. See Figure 7 below for the convergence plot and Figure 8 for the resulting deformed structure.

Figure 7. Convergence plot for the finite element analysis of the frame. The software successfully converged the Von Mises stresses to within 1.1% with a mesh of 128,000 elements.

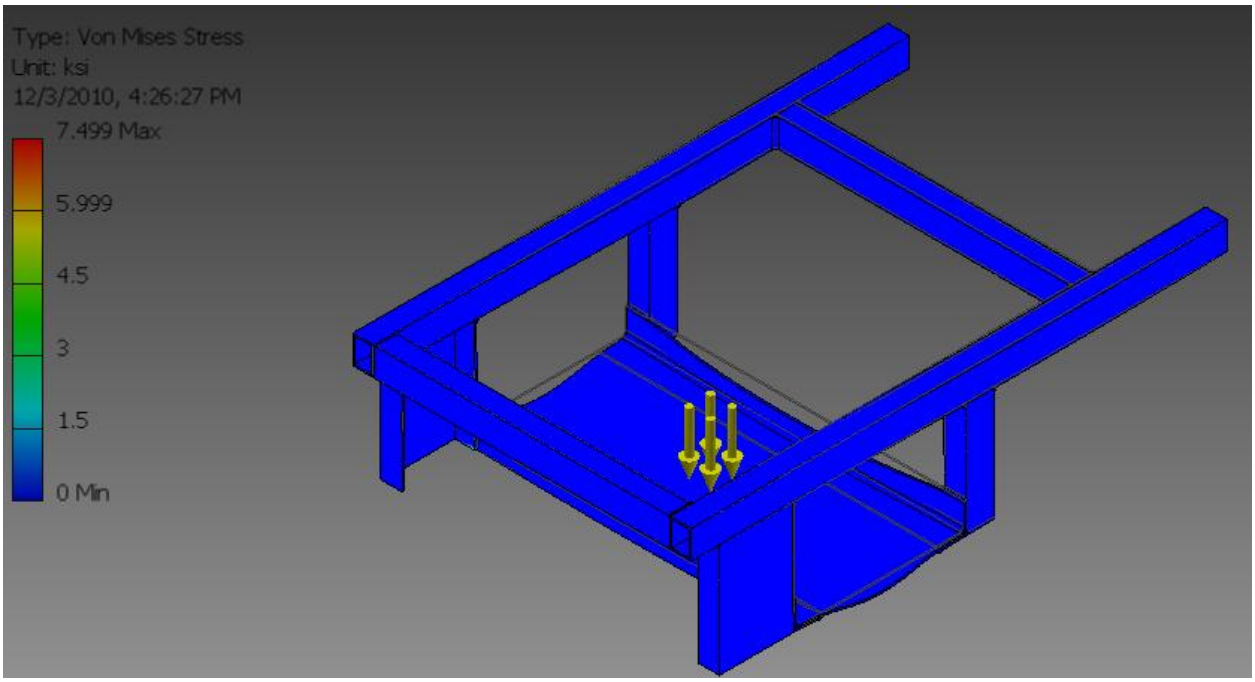

Figure 8. Image of the deformed frame from the FEA. The color gradient represents the Von Mises stresses. The majority of the frame is under minimal stress.

Based on the figure above, the maximum Von Mises stress for this size of material (1/8 inch wall) is 7.5 ksi. It is not easily visible above, but the stress concentration occurs at the welded joints supporting the battery support plate.

According to the results of the finite element analysis, the static stresses experienced by the frame are minimal compared to the yield strengths of commonly available metals like steel and aluminum. Additionally, the maximum stress is concentrated in a small, localized area. This means the worst case scenario is localized yielding, but complete failure is deemed highly unlikely.

Material Selection. Using a 1/8 inch wall material and a 7.5ksi maximum stress, the design team performed a trade-off analysis for readily available materials. In particular, a decision matrix analysis was performed on 1008 Steel, 4130 Steel, 6061 Aluminum and 6063 Aluminum components from McMaster-Carr. Table 4 shows the comparison chart used in the decision process. The effective stress concentration is an analytical number that was created using 7.5 ksi maximum stress seen in the FEA analysis. This max stress was scaled up if the evaluated material's wall thickness was less than 1/8 inch, and this increased stress concentration was used to develop comparative safety factors for the four materials. As seen in Table 4, the

1008 Steel has the highest safety factor; however, the 1008 Steel is also the heaviest of the materials. The Aluminum choices are weaker than the steels, but are also lighter and less expensive.

Table 4. Comparison table for the four selected material choices.

Material	4130 Steel	1008 Steel	6061 Al	6063 Al
Stress Concentration (psi) (based on 0.125" wall, 1"x2")	7500	7500	7500	7500
Wall thickness (in)	0.065	0.12	0.125	0.125
Effective stress concentration (psi)	14423.07	7812.5	7500	7500
Yield Strength (psi)	75000	41335.7	35000	16000
Factor of Safety	5.2	5.29097	4.66666	2.13333
Volume (in3)	97.4272	179.865	187.36	187.36
Density (lb/in3)	0.289018	0.28432	0.09754	0.09754
Weight	28.15824	51.1397	18.2757	18.2757
Price per foot ($/ft)	18.45	5.89	6.20	5.43
Total length	15	18	15	15
Total cost	276.7	106.08	92.95	81.5

The three parameters that the team focused on in the decision process were the factor of safety, weight, and cost. These parameters were assigned normalized scores based on the material that had the most desirable value for each category. For example, the material with the highest factor of safety was 1008 Steel, which was scored a “1”. Each of the other three materials was given a score based on their safety factor’s percentage of the 1008 Steel safety factor. Once the normalized scores were set, each parameter was given a weight out of 100. The factor of safety was considered to have the most importance, and was given a weight of 50. The material weight was given a weight of 40, and the material cost was given a weight of 10. The normalized scores were then multiplied by their respective weights, leaving each material with three weighted scores each. These scores were added up to give the final score for each material. Table 5 displays the normalized scores, parameter weights, weighted scores and final scores for the four materials. The 6061 Aluminum finished with the highest score, and was agreed upon by the design team as the best material choice.

Table 5. Final scores for the four selected materials. Normalized scores were multiplied by the respective parameter weights and added together to give each material's final score.

Normalized scores (0 to 1)				
Material	4130 Steel	1008 Steel	6061 Al	6063 Al
Factor of safety	0.982805	1	0.882005	0.403202
Weight	0.649038	0.3573	1	1
Cost	0.294542	0.7682	0.87681	1
Weighted Scores				
Material	4130 Steel	1008 Steel	6061 Al	6063 Al
Factor of safety (50%)	49.14026	50	44.1002	20.1601
Weight (40%)	25.96153	14.294	40	40
Cost (10%)	2.945428	7.6828	8.76815	10
Total	78.04723	71.977	92.8683	70.1601

Once 6061Aluminum was chosen, the needed materials were priced and ordered from McMaster Carr. Table 6 lists the needed materials to build the frame of the platform, along with the cost for each purchase and the total cost for all materials. The total cost of the frame materials was $326.92.

Table 6. List of materials purchased for building the platform frame.

Item	**Part Number**	**Cost (ea)**	**Quantity**	**Totals**
1x2 6061 Box Tube 1/8" Wall 6' Long	6546K393	$32.05	3	$96.15
2.25x4 6061 Channel 0.19" Base 0.29" Leg 5' Long	1630T18	$55.38	1	$55.38
2x2 6061 Angle 1/8" Thick 8' Long	8982K25	$32.27	1	$32.27
24x24 6061 Sheet 1/8" Thick	89015K48	$71.56	2	$143.12
			Total	**$326.92**

The mechanical platform was constructed of 6061 high strength aluminum. The platform was built of ¼ inch box tubing, 1/8 inch sheet metal, as well as four pneumatic tires, two mounted on ball-bearing casters. The two drive wheels are mounted with bearings ordered from McMaster-Carr through their online division. In house tools were used to cut the box tubing to the correct dimensions, and then these pieces were brought to a local machine shop along with

the full CAD drawings to be welded to our specifications. The team felt that it would be better to contract out the welding due to the team's lack of welding experience with the aluminum.

Drivetrain Design Results. The drivetrain team designed batteries, motors and gearboxes to provide the necessary propulsion as defined in the customer needs. The goal was to select drivetrain components capable of integrating into the final product to provide power and drive capabilities to propel the full mass of the vehicle with a minimum speed of 10 mph on varied terrain. Additionally, the motors were selected to provide the capability of climbing curbs and small obstacles.

Battery selection. After a thorough research on popular battery products on the market, the team found that there were three options in terms of battery types: nickel metal hydride, lithium polymer and lithium iron phosphate. All three batteries have their advantages as well as disadvantages. Nickel metal hydride batteries (NiMH) are the most common batteries as they do not need extensive protection, but they weigh more than most batteries. Lithium Iron phosphate (LIP) and lithium polymer (Li-Po) batteries are very similar in characteristics as they are both light and highly energy concentrated. However, they require constant monitoring during operation as well as cell balancing to achieve its maximum performance.

Before the team decided on the battery type, first a decision was made on the specification requirement for the vehicle battery. Based on the vehicle spec calculation, it was found that in order to drive at 10mph on flat concrete surface; the battery had to provide a 30W power output for each motor. On flat grass surface, the power output requirement for each motor was approximately 150W. Taking into account the effect of inclination, a dynamic scenario was created in which during an 8 hour span, there is 1 hour sitting still, 1 hour running 5 degrees uphill on grass at 10mph, 1 hour running at 5 degree uphill on concrete at 10 mph, 2 hours running on flat grass surface at 10mph and 3 hours running on flat concrete surface at 10mph. The total energy required for this dynamic scenario was approximately 1600Wh. It should be noted that the energy requirement is actually a lot higher for NiMH because it would add at least 30% more weight to the system. As far as Li-Po and LIP are concerned, this necessitates a 2000Wh battery because only 80-90% of the rated capacity can be used before it drops below the terminal cell voltage. It is also worth noticing that the aforementioned dynamic scenario is most likely more intense than what the vehicle would actually experience. However, since factors such as the transmission resistance were not considered in the calculation, good practice requires an over-design to compensate for the lack of reliability in the estimate. Table 7 shows a comparison of the three battery types at 2000Wh. In view of the fact that a light weight vehicle is preferable, NiMH was not the best choice. In consideration of LIP and Li-Po, they present similar traits. But Lithium Polymer comes with a smaller package at a much higher price. Since both require constant monitoring, Lithium Iron Phosphate was deemed the best choice from both an economic and a technical point of view.

Table 7. Comparison of the available batteries used to select the Lithium Iron Phosphate.

Battery Type	NiMH	Lithium Iron Phosphate	Lithium Polymer
Single Cell Dimension(mm)	33(D) x 91 (L)	128 x 66 x 236	280 x 61 x 61
Single Cell Weight(kg)	0.238	2.85	1.7
Single Cell Voltage(v)	1.2	3.2	14.8
Single Cell Capacity(Ah)	13	100	21
Cell Alignment(SerialxParallel)	20x8	8x1	2x5
Current Limit(A)	320	300	150
Pack Volume(L)	15.9	15.9	10.42
Pack Weight(kg)	38	22.8	17
Pack Voltage(V)	24	25.6	29.6
Pack Capacity(Ah)	104	100	105
Approximated Cost($)	2000+	2200	3750+
Protection Circuit Board	NA	Required	Required

Once the Lithium Iron Phosphate battery was chosen, a price quote was requested from AA Portable Power Corporation. Table 8 lists the needed parts along with the cost for each purchase and the total cost. The lithium iron phosphate battery was estimated to cost $2232 and the protection circuit board was estimated to cost $225.95. The total cost of the battery assemble was $2457.95.

Table 8. Battery assembly items and cost.

Item	Part Number	Cost (ea)	Quantity	Totals
Lithium Iron Phosphate Battery	Customized	$2232.00	1	$2232.00
Protection Circuit Board	PCM-LFP25.6V100A	$225.95	1	$225.95
			Total	**$2457.95**

Battery Monitoring. Sheet metal connecters were made to connect cell batteries as is shown in Figure 8. All eight cells were connected in series so that the battery pack has 25.6V nominal voltage. Each cell is also wired separately to the Energy Management System (EMS) so that the cell voltage can be monitored during both the charging cycles and discharge.

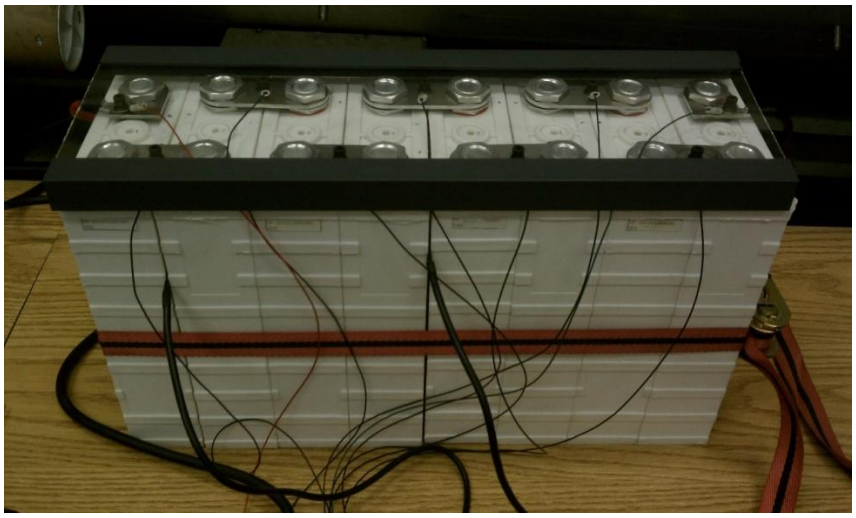

Figure 8. The assembled battery pack with wires connected to the EMS.

The EMS was constructed of four main components: a Central Control Module (CCM), a smart charger, a Data Collection Module (DCM) with two temperature sensors, and a current sensor. Figure 9 illustrates the basic architecture of the EMS. The EMS was structured with a Master-Slave(s) architecture, where the master module CCM manages one or multiple slave module DCMs. Each DCM is capable of monitoring the voltage of up to 12 individual cells, as well as two temperature measurements. Since only 8 cells are needed for this vehicle, only one DCM was installed on the system. An open loop hall current sensor was connected to the CCM. It monitors the current drain of the battery up to 1000A. Using this current and the cell voltage data, the CCM estimates the real time state of charge with the built-in Extended Kalman Filter (EKF) algorithm with an accuracy of 8%-10%. A 3.5 inch LCD touchscreen was purchased with the EMS so that the charging and balancing function can be easily reconfigured.

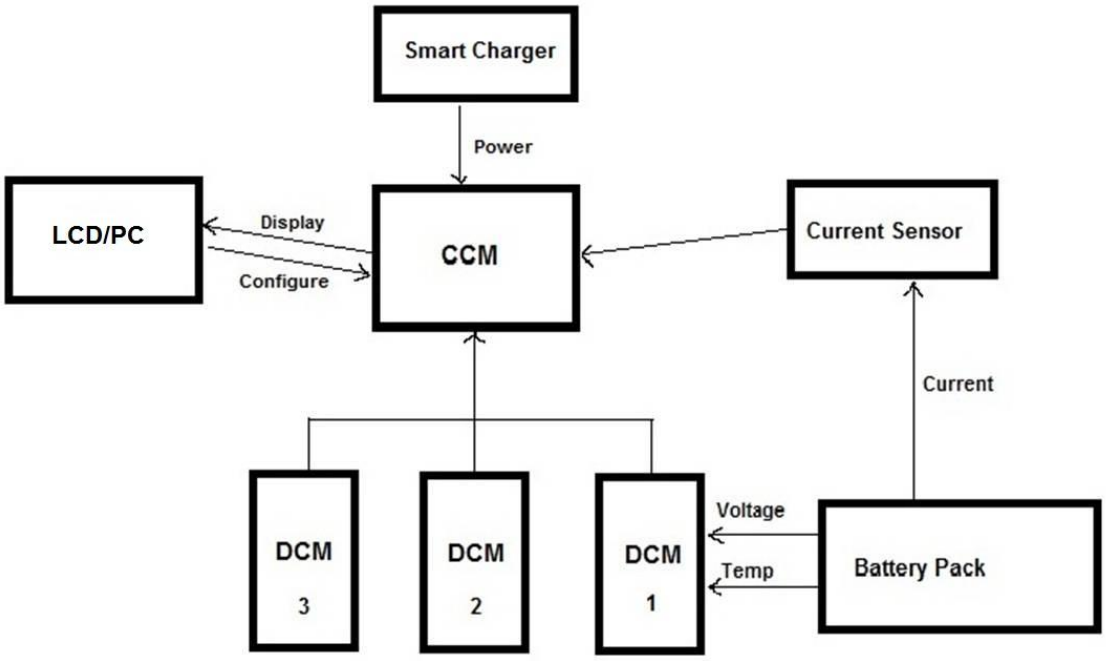

Figure 9. A diagram showing the architecture of the EMS.

During the charging cycles, a smart charger was connected to the CCM to provide electricity for the battery. Using the smart charger, the battery first charges at constant current at a programmable charging current. Then after every cell reaches a predetermined voltage, it charges at constant voltage until it is fully charged. The maximum charging current provided by the smart charger was 40A, but it is possible to connect multiple chargers to the CCM to speed up the charging process.

The CCM also comes with a balancing function, which proved to be crucial for Lithium Iron Phosphate batteries. It automatically balances between the cell voltages so that all cell voltages are within 20-80mV, leading to a higher efficiency.

On the other hand, single cell voltage pose a potential safety problem when over charged, so an overcharging protection range was programmed in the charging function. Currently, the charging process stops when a cell voltage exceeds 3.8V and it does not start again until it drops below the overcharging release voltage. A similar protection was also configured at a lower voltage level. The battery was also protected against overheating by setting an overheat protection temperature. Fortunately, during the a few test runs by far, overheating was not an issue.

Even though the EMS includes a 3.5 inch LCD touchscreen for status monitoring and configuration, a communication interface between the EMS and on-board computer was still essential to monitor the battery status under autonomous mode. The architecture of the EMS makes it possible to replace the LCD touchscreen with a PC terminal and communicate with the

CCM through serial communication. Based on the documents purchased from the EMS manufacturer, the CCM adopted the Modbus-RTU protocol with configurations "9600, 8, No, 1": Baud rate 9600, 8 bits, no polarity bit, and 1 stop bit. A 16-bit cyclic redundancy checksum CRC-16-IBM was attached to the end of each message for error detection. A large amount of measurement data was available from the CCM, and among them the cell voltage, current, state of charge and temperature were of the greatest importance to our vehicle.

Figure 10 shows the Labview interface of the VI. When the user sends a "Battery Pack Information" requests, the CCM returns data such as the total voltage, current, state of charge estimation, cycle count, remaining capacity and so on. When the user sends a "Cell Information" requests, the CCM returns the cell voltage for each of the eight cells. For each request, the 16-bit CRC is checked to confirm whether the received message is corrupted.

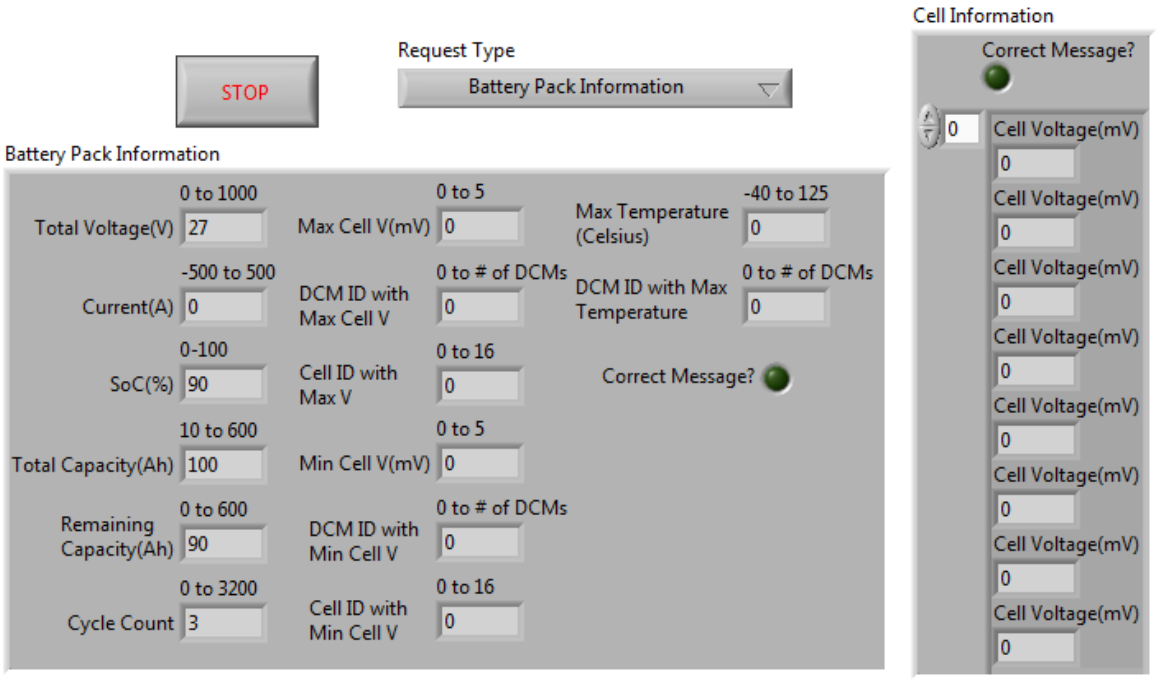

Figure 10. The Labview interface of the EMS communication VI.

A Labview VI was then created to continuously access data from the CCM, including both the battery pack information and individual cell voltages, triggered by user requests. A similar sub-VI was also designed so that the main program can call it anytime and access the battery data. The program was tested on a laptop and was deemed ready for the final implementation.

Battery case design and construction. The battery case was designed to protect the battery and battery contacts from water and vibrations. The case was constructed from 1/8 in. Chemical-Resistant PVC, as it is both weatherproof and electrically insulated. The interior of the

case was lined with 1/8 in. thick foam rubber at the corners and the edges in order to seal the case against water as well as protect the battery contacts from vibrations.

Motor and gearbox selection. The drivetrain design of the vehicle consisted of an assembly that includes a motor, gearbox, and controller. A pair of brushless electric motors were used to drive the vehicle. Gearboxes were used to increase the torque provided by the motors. A controller was used to adjust the current provided to the motor and thus the speed it turns.

The vehicle's performance goals influenced the design and ultimate choice of the motor. The vehicle was required to be able to travel at 10 mph on concrete and climb a curb of 4 inches. To travel at 10 mph, the vehicle required a certain amount of power that is provided by the motors. The power required is given by Equation 1:

$$P = \tau * \omega \tag{1}$$

where P is the power, τ is the torque supplied to the tires, and ω is the angular velocity of the tires driven by the motors. The angular velocity of the tires can be determined simply from the speed requirement.

$$\omega = 2\pi * f \tag{2}$$

$$f = \frac{v}{\pi d} \tag{3}$$

Therefore,

$$\omega = \frac{2v}{d} \tag{4}$$

where f is the frequency of tire rotation, v is the linear velocity of the vehicle, and d is the diameter of the tire. To find the torque required to drive the vehicle, a free body diagram is useful. Because each tire will have its own motor to obtain differential steering, a free body diagram for one tire is shown in Figure 10.

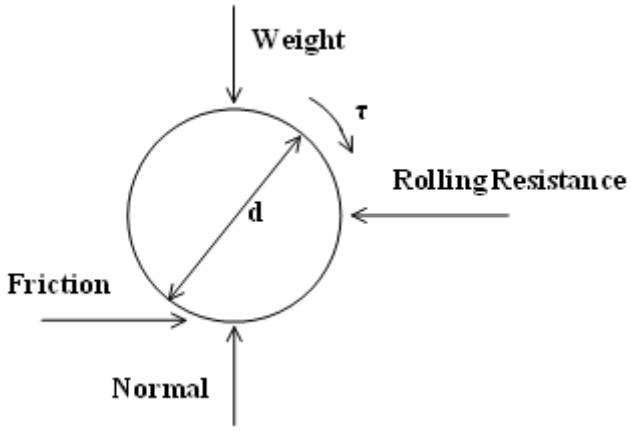

Figure 10. Free body diagram of vehicle tire

Rolling resistance is a resistive force caused by the deformation of a round object rolling on a surface. Rolling resistance, R, can be found from Equation 5:

$$R = C_{rr} * N \tag{5}$$

where C_{rr} is the coefficient of rolling resistance and N is the normal force. C_{rr} has been found experimentally for a variety of cases. For a vehicle with pneumatic tires on concrete, it is estimated to be 0.017. Summing moments about the center of the tire allows the friction to be put in terms of torque, as shown in Equation 6.

$$Friction = \frac{2\tau}{d} \tag{6}$$

Finally, summing the forces on the tire and setting the acceleration to zero, the torque required to sustain a constant velocity is found.

$$\tau = C_{rr} * N * \frac{d}{2} \tag{7}$$

Using a C_{rr} of 0.017, a normal force of 294 N per tire (as estimated by the design team from the mechanical design of the vehicle), and a tire diameter of 12 inches, the estimated torque required is 0.762 N-m. Using a velocity of 10 mph and Equation 4, the required power to operate the vehicle is 33.5 W.

Following this, the design team looked at a scenario of traveling up an inclined plane. The goal was to meet the performance specifications in an extreme scenario. Figure 11 is a free body diagram of this situation.

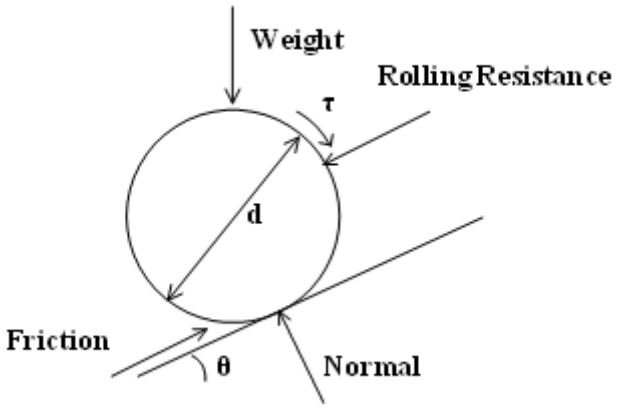

Figure 11. Free body diagram of vehicle tire on a slope

A similar approach was taken to find the necessary torque needed to travel up a five degree concrete incline. The necessary torque to do this is 4.67 N-m. The angular velocity needed for this scenario is the same as on flat ground. Using Equation 4, the power required was found to be 205.4 W. Because this was an extreme but realistic scenario, the drive-train was designed using this power requirement.

With this power requirement in mind, the design team performed a product search. There were three brushless dc motors found that met the power requirement. To decide what motor to purchase, a selection matrix was made. This is shown in Table 8.

Table 9. Selection matrix based on the price, lead time, voltage, and maximum speed on flat concrete.

	Weights (%)	Maxon 136210 (250 W)	Maxon 167131 (400 W)	SM 3450 (500 W)
Price ($)	**25**	**25**	**17.3**	**0**
Max incline on grass (deg)	**25**	**0**	**7.3**	**25**
Lead Time (days till ship)	**5**	**5**	**1.2**	**0**
Voltage (V)	**20**	**20**	**0**	**0**
Max speed on flat concrete (mph)	**25**	**16.7**	**25**	**0**
	100	**66.7**	**50.8**	**25**

The selection matrix was based on the price, lead time, voltage (24 V was preferable due to safety), maximum incline and maximum speed on flat concrete. After considering the selection matrix, it became clear that the 250 W motor was the better motor choice. The motor had no problem meeting specifications, including the extreme scenario of traveling up a 5 degree incline. It also was more readily available, cheaper, and safer (because it operates at half the voltage) than the 400 W Maxon motor and the 500 W smart motor.

It was determined to purchase the 250 W Maxon motor. It operates at 24 V, has a nominal speed of 9090 rev/min, and nominal torque of 0.285 N-m. Using a gearbox ratio of 27:1, the output angular velocity and torque became 35 rad/s and 7.7 N-m respectively. This allowed the vehicle to travel at a top speed of 12 mph and up a maximum incline of 9 degrees. It was also able to produce a maximum torque of 113 N-m for very short periods of time.

In order to climb a curb, the drive wheels were required to be able to lift whatever fraction of the vehicle weight they carry. We can analyzed this requirement by forming a simplified model of the frame design, seen in Figure 12. In this design, the front wheels are the driving wheels and are 12 inches in diameter. The weight is distributed in such a way that it is 2/5 of the way from the front of the frame.

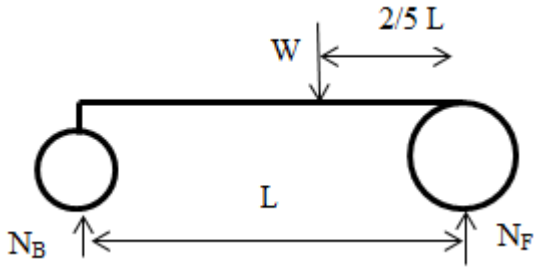

Figure 12. Free body diagram of vehicle frame. W is the weight including batteries and motors, L is the length of the vehicle frame from axle to axle, and N_F and N_B are the normal forces on the front and back wheels respectively.

Summing moments about the back wheel, it was seen that:

$$\frac{-3W}{5} * L + N_F * L = 0 \tag{8}$$

where W is the weight including batteries and motors, L is the length of the vehicle frame from axle to axle, and N_F and N_B are the normal forces on the front and back wheels respectively. Solving for N_F.

$$N_F = \frac{3W}{5} \tag{9}$$

So the front wheels supported three fifths of the total vehicle weight. If this wheel approached and attempted to climb a curb, the wheel's free body diagram would resemble Figure 13. Each wheel in the front would have carried half of the front-load, resulting in 3/10 of the total weight. At the instant the wheel raises off the ground, no normal force would be pressing on the vehicle from the ground.

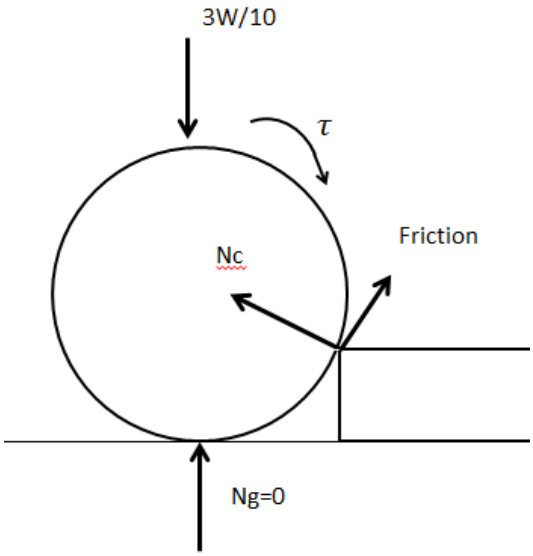

Figure 13. Free body diagram of a front wheel climbing a curb.

It is convenient and reasonable to assume the front wheels would not slip while climbing the curb, allowing the summation of moments around the point where the wheel contacts the curb. By summing moments about this point, it was possible to disregard the friction and normal force from the curb, as seen in Figure 14.

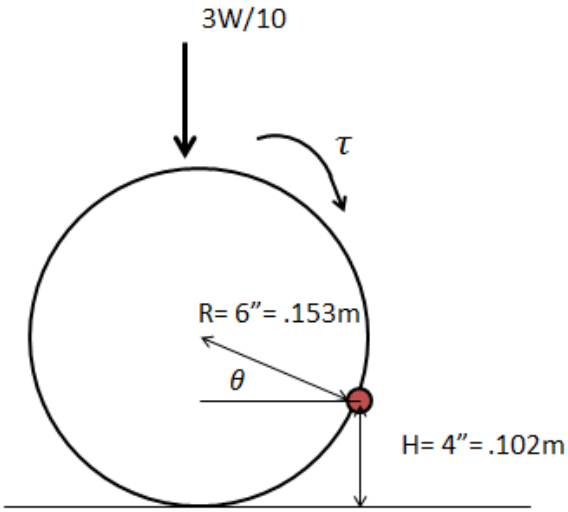

Figure 14. Free body diagram with relevant components for summing moments at the curb contact point.

Making these assumptions,

$$\frac{3W}{10} * \mathrm{R}\cos(\theta) - \tau = 0 \tag{10}$$

The center of the circle is R-H above the point of contact, meaning that

$$\sin(\theta) = \frac{R - H}{R} \tag{11}$$

where R is 6 inches, and H is 4 inches

$$\theta = \sin^{-1}\left(\frac{1}{3}\right) = 19.5° \tag{12}$$

Relating this information back to Equation 10 and using an estimated weight of 588N (60kg),

$$\tau = \frac{3 * 588N}{10} * .152\mathrm{m} * \cos(19.5°) = 25.3\,Nm \tag{13}$$

So any motor capable of supplying 25.3 Nm of torque to the wheels would be able to climb a four inch curb. The 250 W Maxon motor that was selected earlier has no problem supplying this torque. The maximum stall torque for this motor was 113 N-m.

A price quote was requested from Maxon for the 250 W Maxon motor along with gear head. Table 9 lists the motor and gear head cost. Each Maxon motor was $673.30. The gear head was $603.70. Buying an assembly for each drive wheel, the total cost was $2554.00.

Table 10. Motor and gear head cost.

Item	Part Number	Cost (ea)	Quantity	Totals
Maxon Motor	EC 45 136210	$673.30	2	$1346.60
Gear Head	GP62 110502	$603.70	2	$1207.40
			Total	**$2554.00**

Motor Control and Feedback

Because Maxon does not supply motor controllers capable of taking advantage of the full capacity of the EC 45 250W motors, several other suppliers were contacted. While power handling capacity was the principal metric for choosing a suitable controller, compactness, feedback support, and ease of computer interfacing were also considered. A pair of single channel Roboteq BL1500BP brushless DC motor controllers were chosen for our application.

Although the decision was made previously to forgo the inclusion of integrated incremental quadrature encoders by the factory in the drive motors, it was later decided to

include the encoders. Because retrofitting of the motors would be time consuming and expensive, E6 encoders from US Digital were selected and fitted to the output shaft of the gearbox. The E6 line was among few that supported such a large shaft diameter, and fit cleanly into our existing design without modification or clearancing. Encoder support was added to the BL1500BP motor controllers through the addition of a Roboteq Encoder Support Add-on Board.

Sensor Suite Design and Selection

IR Camera Selection. The autonomous ground vehicle required an infrared imaging camera to provide a visual representation of heat radiated by surroundings. Furthermore, the thermal infrared imaging camera was used to see under adverse conditions, in the dark, through fog, and through heavy smoke. The infrared camera sensor was designed to be mounted on the top of the platform at a position and angle where blind spots are minimized.

The market has a large selection of thermal imaging camera sensors. In order to choose the best camera for our applications, the IR cameras were evaluated by size, weight, power consumption, field of view, lead time, price, and interface type and capability. After some research, it was concluded that the infrared cameras made by FLIR had an outstanding performance compared to what was available in other markets.

Two infrared camera models from FLIR were compared and evaluated. The first IR camera looked at was the Photon 320 seen in Figure 15. The Photon 320 is 51.4 x 49.8 x 34.0 mm in size and weights 97g. It has a power consumption of less than 3 Watts and an optimal field of view of 46^{o}x36^{o}. Finally, the Photon 320 had a price of $6,600.

Figure 15. FLIR Photon 320 Uncooled Core Thermal Infrared Camera

The second IR camera that was looked at was the Tau 320 shown in figure 16. The Tau 320 is 44.5 x 44.5 x 30.0 mm in size and weights 72g. It had a power consumption of less than 1 Watt and an optimal field of view of 48^{o}x37^{o}. Finally, the Tau 320 had a price of $6,500. Both the Photon 320 and Tau 320 had a lead time of two weeks. After comparing the two IR camera models, the team concluded that the Tau 320 had a better performance in all criterions.

Figure 16. FLIR Tau 320 Uncooled Core Thermal Infrared Camera

The FLIR uncooled core thermal imager Tau 320 was selected with a 9mm lens for wide field view and video output module. The IR camera was selected so that it could be controlled for triggering and configured via USB and LabView interface. Also, the Tau 320 had an analog video output which needs the use of a separate frame grabber.

In summary, the FLIR Tau 320 infrared camera was selected since it was small size, light weight, had very small power consumption, and had outstanding imaging performance. The support of the Tau 320 required a USB frame grabber evaluation and LabView Interface development. Figure 17 shows a sample picture collected by the LabView program developed specifically for the IR camera. The program was capable of capturing both pictures and videos.

Figure 17. FLIR Tau 320 sample data.

LIDAR Sensor Selection. Obstacle detection and avoidance in autonomous systems requires the ability to accurately determine the location of free paths and obstructions relative to

the autonomous vehicle's current location. Optical systems are typically favored over acoustic systems due to their relative accuracy and resolution. Stereovision systems work by observing the environment from multiple perspectives and using parallax between the multiple sensors to discern the location of common feature points between images. This can lead to accurate distance data, but requires high level image processing and comparisons between images. Typically, the easiest and most accurate way to detect the location of path obstructions is through direct measurement using Light Detection and Ranging (LIDAR). LIDAR sensors use time of flight data from pulses of emitted infrared radiation (typically from a laser pulse) to calculate the location of the nearest surface within the sensor's range.

The use of LIDAR in autonomous vehicles is well documented and standard practice for most applications. A line-scanner is usually placed on the front of the vehicle to generate a two dimensional occupancy plot of the sensed obstructions. A standard line-scanning LIDAR will be used for navigation and obstacle avoidance, but because this autonomous vehicle will be used to generate three dimensional mapping data, it was necessary to explore the LIDAR market for unique sensors capable of collecting distance data in both horizontal and vertical fields of view.

Several novel sensor types have recently become available on the market for this purpose and have been selected for evaluation. The three new emerging technologies are: multi-plane scanners, 360° three-dimensional LIDAR, and flash LIDARs (3D cameras). Because this vehicle is being used as the prototype for several vehicles, it is unlikely that all of the following sensors will be equipped on a single vehicle, but this first vehicle will be used as a testbed for each of the purchased sensors to determine which will be of most use for future vehicles.

The first type of multi-dimensional scanning LIDAR is simply a multi-plane LIDAR capable of scanning in a line at the horizontal as well as a line located a few degrees above or below the horizontal. Two essentially identical sensors of this type are available. One is produced by the SICK Group, and the second is produced by IBEO. The important parameters that characterize these sensors can be seen below in

Table below.

Table 11. Comparison between the IBEO LUX and SICK LD-MRS multi-plane LIDAR sensors.

	SICK LD-MRS	IBEO LUX
Range	250m	200m
Range for 10% reflective surface	30m	50m
Layers	4	4
Angular Resolution	.125 degrees	.125 degrees
Field of View	85 or 110 deg	85 or 110 deg
Object Classification?	no	yes
Multiple returns?	3	3
Distance Resolution	4 cm	4 cm
Cost	$20,267	$18,753

Because this vehicle was designed to move at only 10 miles per hour, the increased range of the SICK LD-MRS was not particularly useful. Additionally, the Lux was capable of on-board processing for object classification (ground, clutter, valid) a feature useful for autonomous navigation. The Lux was also a sensor which has been used very successfully on the "Blind Driver Challenge" at Virginia Tech, giving this team a valuable resource when integrating the sensor. Because of the additional on-board processing, coupled with a reduced cost and local experience with the IBEO, the Lux was selected over the SICK for the multi-plane scanner.

The second new technology is a rotating, multi-beam LIDAR capable of generating a full 360° point cloud in dozens of planes over up to a 40° vertical field of view. This technology is being pioneered by Velodyne in their HDL-64E and HDL-32E High Definition LIDAR sensors. The HDL-64E was the first generation sensor, capable of collecting 1.3 million points of data per second from 64 beams over a 26.8° vertical field of view. Being a first generation sensor, however, the 64E was a large (~30 lb) sensor with a $75,000 price tag, making it both too large and expensive for our purposes.

The 32E was Velodyne's response to an increasing demand for a lighter and cheaper sensor. The 32E produced 32 beams of data over a 40° vertical field of view at a data rate of 800,000 points per second. It functioned by scanning as the entire unit (seen in Figure 7) rotates at a user defined rate of 5-20Hz and was capable of sensing multiple returns per pulse allowing it to see through dust, fog, and potentially foliage. Being a second generation sensor, the 32E was significantly cheaper than its predecessor with a price of $29,900 and a weight of ~4lbs making

it ideal for our small vehicle. The high data rate and wide field of view was ideal for the intended research in both three dimensional mapping and compressed sensing.

Figure 17. Velodyne HDL-32E Three-Dimensional LIDAR.

The third type of emerging LIDAR technology that was evaluated was a Flash LIDAR sensor. While the previous sensors worked using precise beams of infrared laser to precisely determine individual points in space one at a time, a flash LIDAR functioned by emitting a more diffuse flash of light and measuring the time of flight data and light intensity on a CCD-like sensor. The resulting data was essentially a pixel array of point cloud coordinates giving a three dimensional snapshot of the environment. The Flash LIDAR was produced by two major companies, the Mesa Imaging *SwissRanger* and the Advanced Scientific Concepts *TigerEye*.

The two sensors differed primarily in the method of light production. The TigerEye used an infrared laser with a diffuser to emit a controlled and intense beam of radiation which was then detected after it returned to the camera sensor. Because of the controlled emission of radiation in laser pulses, the ASC product was capable of multiple returns as well as ranges in excess of 100m depending on diffuser and lens chosen. However, this technology was still in the early stages of development and had a $150,000 price tag attached. It was consired a more viable alternative in 5 years or so after several generations of refinement allow for the production of cheaper models.

The SwissRanger, by comparison is a low-range (~10m) sensor which used a diffuse flash of infrared light to illuminate the surrounding area and produce a 176x144 pixel array of point cloud data. This sensor was a fourth generation model and had a significantly lower cost of only $9,095. This sensor was compact, lightweight, and perfect for obtaining a 3D data at camera-like frame rates of 50fps. This sensor was also cheap and ideal for integration with a vision sensor as discussed later in this report to produce life-like 3D color representations of the environment.

In summary, to test the emerging technologies of multi-plane LIDAR, rotating 3D LIDAR, and 3D TOF cameras (Flash LIDAR) in an autonomous 3D mapping scenario, this design team determined the IBEO Lux, Velodyne HDL-32E, and Mesa Imaging SwissRanger

were the ideal sensors for integration with this type of mapping vehicle. After the sensors were received and fully tested, recommendations were be made on which would be most useful for use on additional mapping vehicles.

Vision camera selection. In addition to rotating a LIDAR unit to perform 3-D mapping, a vision camera was used to provide a baseline measurement against which to calibrate the various point cloud sensors. Therefore, the design team performed a search of vision cameras to determine the best product to use. Cameras were inspected based on various criteria and from many companies, including National Instruments, Videre, Pointe Grey, Sony, and Basler.

The first performance parameter we examined was the shutter speed, or exposure time, of a camera. The exposure time indicates how long the lens stays open to take in light for each frame. An exposure time that is too long will result in blurry images due to objects moving across the pixels of the lens during the exposure. Because the camera would be rotating with the LIDAR sensor relatively quickly, a short exposure time was deemed imperative. Additional analysis was done to determine how short the exposure time must be.

As stated above, the Swiss Ranger was identified as the desired LIDAR sensor early in the sensor selection phase of the project. In order to perform the selection of the vision sensor, a few simple dynamics equations were developed to equate optical sensor specifications to overall platform performance. Particularly, the equations provide a quantitative analysis of manufacturer specified frame rates, resolutions, fields of view and shutter speeds. The results provide a measure of the frames collected in each revolution and the pixel shift during shutter opening. This allows for prediction of the angular speed that will lead to missing data and image blur. The limiting angular velocity for missing data was calculated as,

$$\omega_{\mathbf{data}} = \frac{\mathrm{FPS} * \mathrm{HFOV}}{360°}$$

where $\omega_{\mathbf{data}}$ is the maximum angular velocity in Hertz, FPS is the frame rate of the camera in frames per second, and HFOV is the horizontal field of view in degrees. This limit provided the maximum angular velocity to ensure that portions of the 360° environment were not missing from the data. The maximum angular velocity for image blur was calculated as,

$$\omega_{\mathbf{blur}} = \frac{\mathrm{HFOV}}{r_H * 360° * t_s}$$

where ω_{blur} is the maximum angular velocity in Hertz, r_H is the horizontal resolution in pixels, and t_s is the shutter speed in seconds. This equation provided the maximum angular velocity to ensure that the optical sensor did not shift more than a single pixel while the shutter was open.

The resolution and frame rate were also important parameters for the camera selection. These two criteria had an inverse relationship with many cameras. Cameras with high resolution had lower frame rates and vice versa. Because our vehicle only used vision for reference to archival data, and not for navigation, an extremely high resolution (e.g. high definition) was not necessary. The frame rate needed to compare well to the LIDAR sensor for effective syncing of images.

The Basler scA640-70gc Scout Machine Vision Camera was chosen and ordered. This camera offers a 659x490 resolution at 71 fps. The resolution was sufficient for our needs, and the frame rate exceeded that of the Swiss Ranger. The camera had a minimum exposure time of 0.02 ms and was programmable by those increments. Although the camera was likely not to be used at that shutter speed, it was tested to achieve a balance for brightness and no blurring. Figure 18 shows the Basler Scout camera without an additional lens.

Figure 18. Basler Scout Machine Vision Camera

The Basler camera was quite small. It weighed 150 grams, had a volume of 94 cm^3, and consumed only 3 watts of power. Therefore, the additional load the camera had on the vehicle was extremely small. Also, there were no issues with its size for mounting the camera for rotation.

One of the most beneficial aspects of the Basler camera was its compatibility. The camera offered a gigabit Ethernet interface, which was compatible with many slip rings. The camera was compatible with NI Vision Acquisition Software, which allowed for simple LabVIEW integration. Because every sensor was integrated into LabVIEW, additional time was

not spent working with the less compatible sensors. Because many of the vision cameras available offered similar specifications in other categories, the Basler's unique compatibility with LabVIEW was a major benefit.

To best match the Scout's images with those taken from the Swiss Ranger, a new lens was purchased. The lens has a 3.5 mm focal length, which allowed the camera to achieve a field of view similar to that of the Swiss Ranger's (69° h x 56° v)). This allowed us to fully take advantage of the 3D sensor. All point cloud data was matched with visual pixels for effecting mapping.

A LabVIEW VI was created that allows for many of the necessary functions to use the camera. Running the software allowed the user to edit a variety of parameters of the camera attributes and acquire images. These parameters includeed gain, shutter speed, frame rate, and color balance ratios. The software saved each image acquired as a bitmap with a filename detailing the test name along with timestamps that were used to reference the image to a LIDAR point cloud. Archival settings allowed for camera data to be saved as compressed or uncompressed images and videos. Additionally, a LabVIEW VI was made that simultaneously acquires images from both the Swiss Ranger and the Basler Scout. Both sensors obtain images with a triggering process in sequence. Therefore, the largest gap between the two images was roughly equal to the exposure time of the camera. This allowed us to easily match point cloud data with the visual image for every frame of operation. The software included many adjustable settings for performance and processing as well. The LIDAR data was processed by a variety of filters. The image outputs were also turned off to increase performance during vehicle operation.

3D Mapping Sensor. In order to complete the project goal of 3D mapping to support distributed sensing research, a 3D mapping platform was developed. The purpose of the platform was to provide point cloud range data with matching optical data to form a 3D perception of the environment in proximity to the vehicle. This was accomplished with two sensors. First, the Swiss Ranger was selected during the LIDAR selection process to be integrated into the 3D mapping platform. Second, a selection process was performed to identify a suitable optical sensor to collect data parallel to the Swiss Ranger. Finally, the platform integrated both sensors into a modular unit that can provide continuous rotation for data collection in all directions. See Figure 19 below for an initial rendering of the platform design.

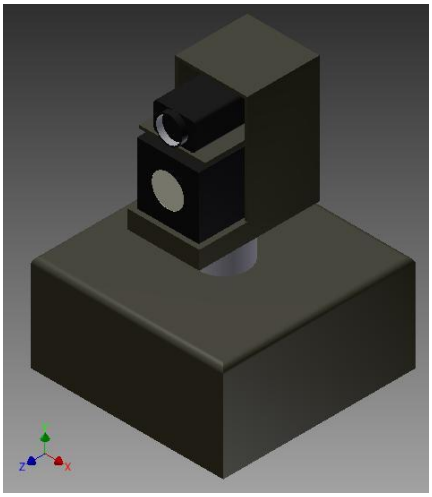

Figure 19. Initial 3D mapping platform design. The platform integrated the Swiss Ranger flash LIDAR and an optical sensor onto a continuously rotating mechanical platform to provide a modular sensor package for 3D mapping and distributed sensing research.

In order to provide continuous 3D mapping, the sensor platform consisted of a slip ring, bearing components, gears, a dc motor, encoder and motor controller. The first component of interest was the slip ring. In order to transmit power and data between the rotating sensors and the stationary base, a slip ring was utilized. The slip ring selection was performed primarily based on the need for particular protocols and data rates.

Slip Ring Selection. The VT-MAGV was selected as a rotating module on the sensor platform. This rotating module allowed the Swiss Ranger Flash LIDAR and the Scout camera to rotate 360 degrees while collecting data. A slip ring was needed to provide a wireless transfer of power and signals to and from the rotating sensors. The slip ring needed to be able to transfer sufficient power for both the Swiss Ranger and Scout camera, as well as triggering signals for both. The slip ring also needed to handle USB 2.0 and 1000 Mbps Ethernet data transfer. Slip rings can be manufactured with brass rings and graphite brushes, or made with precious metal rings and brushes such as silver or gold. Resistance in slip rings can lead to electrical noise and voltage drop across the rings. Slip rings with precious metal contacts are more expensive, but provide low and consistent resistance. Since low noise is an important consideration for transferring the Swiss Ranger and Scout data, the design team began a market search for precious metal slip rings.

The limiting factor in the market search was USB 2.0 capability. Multiple slip ring manufactures were contacted, and only two commercial manufacturers were confident in their product's ability to handle USB 2.0 data transfer. Those two companies are IEC Corp. and Electro-Miniatures Corp. The slip ring market search was then narrowed down to the models from each of these two companies that best met our requirements. Figure 20 shows the Model 2175 from Electro-Miniatures. The Model 2175 had gold-on-gold contacts and was rated for a

maximum noise level of 5 mΩ. The Model 2175 contains 40 circuits and supported a maximum current of 1 A per circuit. The Swiss Ranger and Scout camera required only 16 circuits, but power transfer was needed at greater than 1 A. If the Model 2175 slip ring was purchased, some of its circuits needed to be combined to obtain the desired power transfer. No official sales quote was acquired for the Model 2175, but a ballpark figure of $2300-$2400 was given to the design team.

Figure 20. Picture of the Model 2175 slip ring manufactured by Electro-Miniatures Corp.

Figure 21 shows a BXSN-type slip ring from IEC Corp. The BXSN uses silver contacts and is rated for 2 mΩ noise. The BXSN can be manufactured with 20 rings that can meet our amperage requirements for power transfer, and has been quoted by IEC at $3,200 per unit.

Figure 21. Picture of a BXSN-type slip ring manufactured by IEC Corp.

The team received a drawing from IEC Corp. of the slip ring they were prepared to build for our purposes, which is shown in Figure 22. The slip ring is 4 inches in diameter and 10.5 inches long. The BXSN slip ring was purchased from IEC Corp. and incorporated into the 3D mapping

designs. Initial testing of the IEC slip ring's performance indicated that the slip ring was capable of transferring USB 2.0 data.

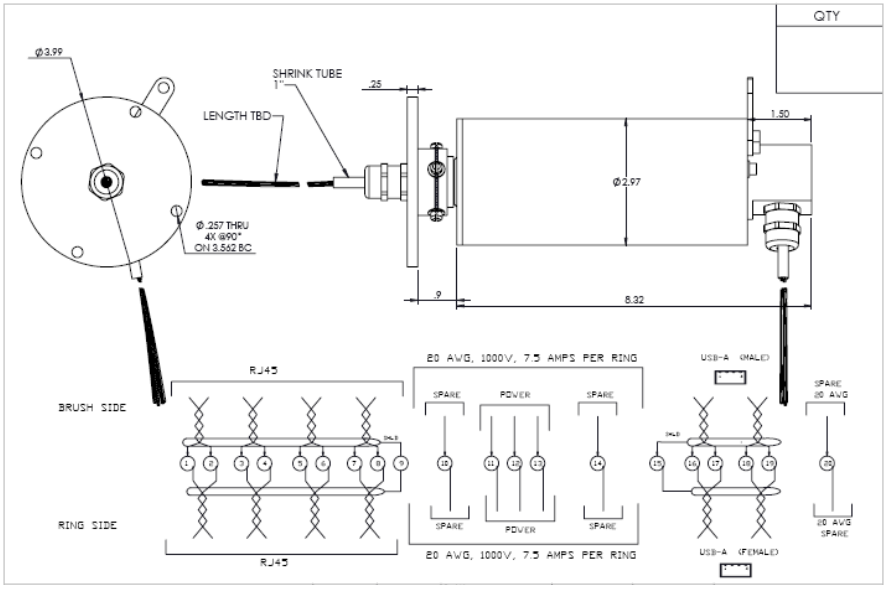

Figure 22. Drawing of desired BSXN-type slip ring from IEC Corp.

The two sensors and the slip ring were selected for the 3D mapping sensor. The remaining tasks involved the mechanical design of a bearing and drive assembly to include gearing, a motor and encoding. Currently, the bearing assembly is under development. Once the bearing assembly is completed, an appropriately sized motor will be selected along with a matching controller and encoder. The final integrated system will provide a modular 3D mapping platform that will be attached to the vehicle.

3D Platform Mechanical Considerations. Due to the light weight and small size of the sensors, the primary mechanical concern was not load or stress. Rather, the driving constraint was the need for a large inner bore through the mechanical components for the wiring of the slip ring. An industry search led to the selection of a polymer plain bearing in the form of a slewing ring. The slewing ring provided a bearing with a large inner bore at a very cost effective rate compared to ball bearings and other methods. After the bearing was selected, the drive system was developed.

Based on readily available components, two options were suggested: a geared drive and a belt drive. Both options could be assembled quickly from off the shelf parts, but the belt drive proved superior for the purposes of the sensor platform. Because the purpose was to rotate sensors, the primary concern for the drive system was minimal kickback and smooth rotation. Both options provide smooth rotation, but a belt drive provided superior performance by eliminating kickback in the drive system. Kickback describes the looseness or tendency of a geared system to be able to shift slightly without actually rotating the gears. Finally, a belt driven

system resulted in reduced tolerances on fabrication. See Figure 23 below for the CAD model of the belt drive system and a photo of the assembled device.

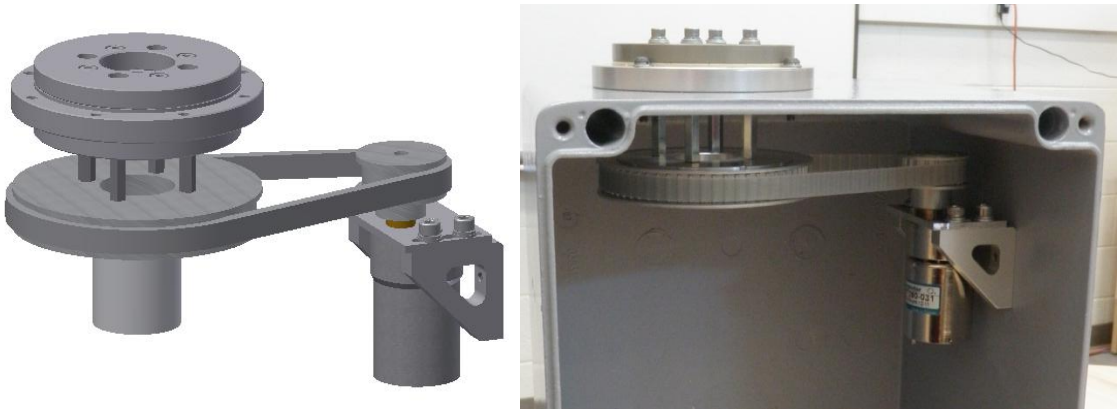

Figure 23. *Left:* CAD model of the belt drive system and bearing. *Right:* Assembled slewing bearing and belt drive.

A simple gear motor was selected and purchased to drive the belt system and rotate the sensors. A controller was also selected, to provide easy control of the rotational speed of the sensor platform. The Pololu Jrk 21v3 controller was purchased based on its simplicity and easy interface. A program was written in LabVIEW that sends commands through the computer's serial port to the Pololu controller, and allows direct control of the gear motor speed. The front panel of this program is shown in Figure 24 below. The program allowed for simple control of the motor speed, and provided the option of reversing the motor's direction.

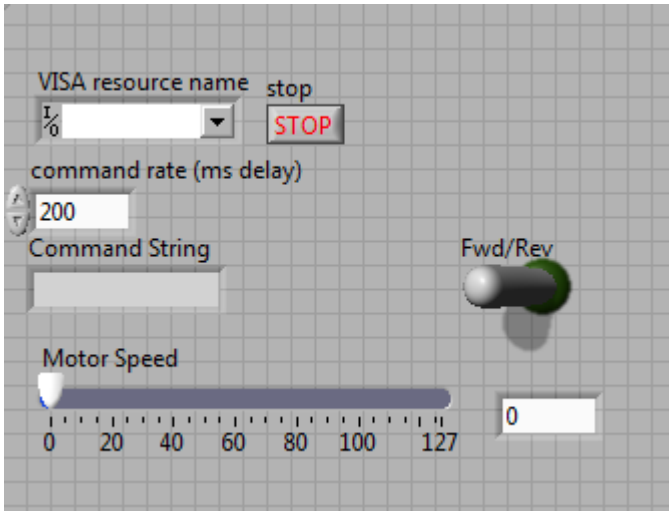

Figure 24. Front panel of the LabVIEW program written to control the gear motor speed. The program allows for easy control of the 3D mapping sensor's rotational speed, and gives the option to reverse rotational direction if necessary.

3D Platform Angular Measurement. A key factor in developing the sensor platform was the capability to accurately measure the angular position of the sensors during data acquisition. This allowd the point cloud data and photos to be mapped accurately relative to the vehicle. In order to achieve accurate measurement of the angular position, the standard industry sensor was a rotary encoder. Rotary encoders mount to rotating shafts and provide highly accurate measurement of rotation. As before, the driving factor in selecting the encoder was the relatively large inner bore. This led to the selection of the 775 model from EPC Encoders. See Figure 24 below for the encoder model as well as the actual mounted encoder. In the photo, note the small silver ring mounted to the shaft. The shaft and silver ring rotated with the assembly, while the remainder of the assembly remained stationary. Inside of the encoder, 4096 counts or pulses were generated per revolution.

Figure 24. *Left:* CAD model of the 775 rotary encoder from EPC. *Right:* Assembled encoder complete with the rotating shaft and a stationary mounting bracket. The shaft inserts into the pulley, which can be observed in the CAD model of Figure 23.

3D Platform Completed Design. The components of the platform were assembled into a cast aluminum enclosure for structural support and protection from the weather. The sensors were selected to be mounted to the bearing with custom-machined aluminum plates. Figure 25 below shows the final CAD model alongside the current fabricated components. Once the assembly is fully functioning, weatherproof bulkhead electrical connectors will be added and the enclosure will be sealed. The final cost of the sensor platform is approximately $4,500 while the sensors themselves total $10,000.

Figure 25. *Left:* CAD model of the final assembled sensor platform. *Right:* Current status of the fabricated platform. The slip ring, rotary encoder, belt drive and bearing are assembled. The sensor mount, slip ring mounts and sensors must be added to complete the assembly. Additionally, bulkhead electrical connectors will be added so the enclosure can be sealed.

GNSS + Inertial Navigation System

An important factor in meeting the navigation and localization goals for this project was the inclusion of a suitable inertially-aided GNSS receiver that was compatible with the Trimble BX960 RTK base station that was owned by the Virginia Tech VAL. Because of the excellent performance of the Trimble-based systems that were tested in the past, the Trimble subsidy Applanix was initially contacted for available systems. The lowest cost, turnkey Trimble/Applanix the POS LV 210 far exceeded the performance requirements of the project. However, the price at $42,000 was in excess of our budgetary restrictions.

Additional turnkey GNSS+INS systems were evaluated, including the Sepentrio AstRx2i and the Novatel SPAN-CPT. Both were fully capable of high-performance RTK positioning in conjunction with the Trimble base station. While neither unit approached the dead-reckoning performance of the Trimble, which integrated a military-grade IMU, both were considerably less expensive. The Sepentrio unit, at $14,000, integrated a lower-quality, off the shelf xSens IMU providing only 0.5 deg of heading and orientation accuracy, while the Novatel SPAN-CPT was capable of an order of magnitude better performance for $23,000, as well as superior sensor

fusion algorithms providing a much more robust state solution. The Novatel SPAN-CPT system was selected.

Sensor Integration

Swiss Ranger and Visual Camera Integration

After receiving the SwissRanger, considerable effort was spent integrating the sensor using the provided application programming interface (API). Although MesaImaging states that LabVIEW was not a supported interface, they also reported that several customers have had great success in integrating the sensor with LabVIEW by utilizing the "Call Library" node to communicate with the SwissRanger function list. Research into this method of sensor control yielded some initial successes in locating and communicating with the API, but several problems essentially left any test programs crippled. In attempting to find someone who had successfully integrated the SwissRanger into LabVIEW, the team stumbled upon a small book: *3D Imaging for Autonomous Robots: Improving Machine Vision Using Time-of-Flight Cameras* by Omer Ecevitoglu. This text outlined a simple LabVIEW interface which could access IR reflectance as well as 3D point cloud data and process this information to achieve some basic feature point detection. The portion of the code outlined below is based largely on the methods outlined by Ecevitoglu, with appropriate modifications and simplifications made to suit the purposes of this particular project.

The front panel of the LabVIEW code consisted of two main panels: Graphs and Settings. The readouts tab only contained data relevant for error checking and troubleshooting. The graphs panel shown in Figure 26 displays three different images as seen by the SwissRanger. In the top right, the plot displays the amplitude of the IR reflectance, producing essentially a black and white image typical of near infrared cameras. The top right is a distance plot which color codes the individual pixels as a function of the Z-distance from the camera. The bottom left plot is a confidence map, which displays how confident the SwissRanger is in its distance information based on variations in the IR reflectance amplitude and the distance images over time. The bottom right window displays the visual spectrum images currently being gathered by the Scout camera. When fitted with the correct lens, the Scout image should match closely with those collected by the flash LiDAR.

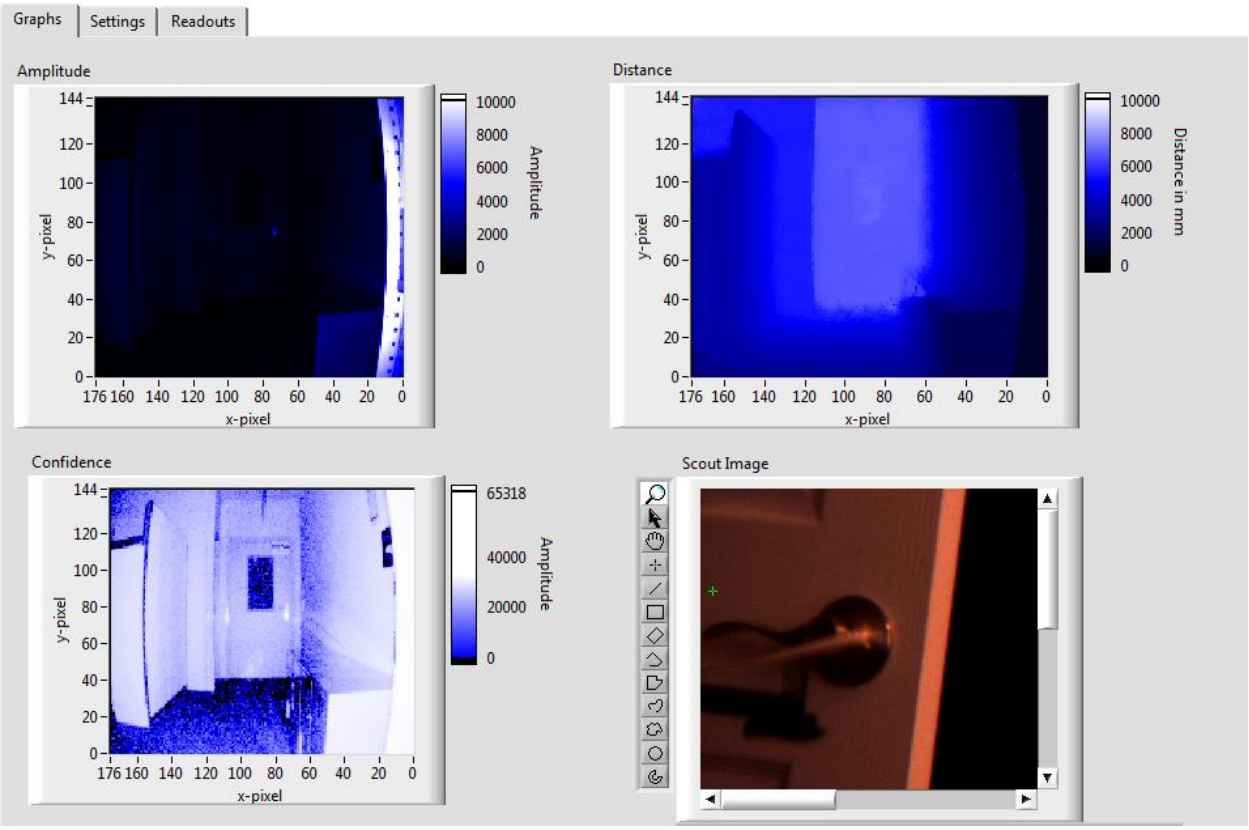

Figure 26. Front panel "Graphs" tab. Contains plots of the IR reflectance amplitude (top left), Z-Distance (top right), Confidence (bottom left), and visual spectrum images (bottom right).

The second tab, "Settings" can be seen in Figure 27. This panel provides a number of useful features of both the SwissRanger and the Scout Camera which can be turned on or off depending on current needs. Either sensor can be activated or inactivated depending on preference. Additionally, the graphs can be turned off to increase data processing rates. If the SwissRanger is not attached via USB, a selection menu allows the user to call up a set of sample data for offline software development. In addition to deactivating the individual sensors, the VI allows the user to set the data collection rate and control whether or not this data is logged. Beyond these basic commands, this tab provides the option of manually setting the Scout camera's gain and exposure rate as well as turn on various filtering options (3x3 median, 5x5 hardware adaptive, gray scale amplitude conversion, and activation of the confidence map) for the SwissRanger.

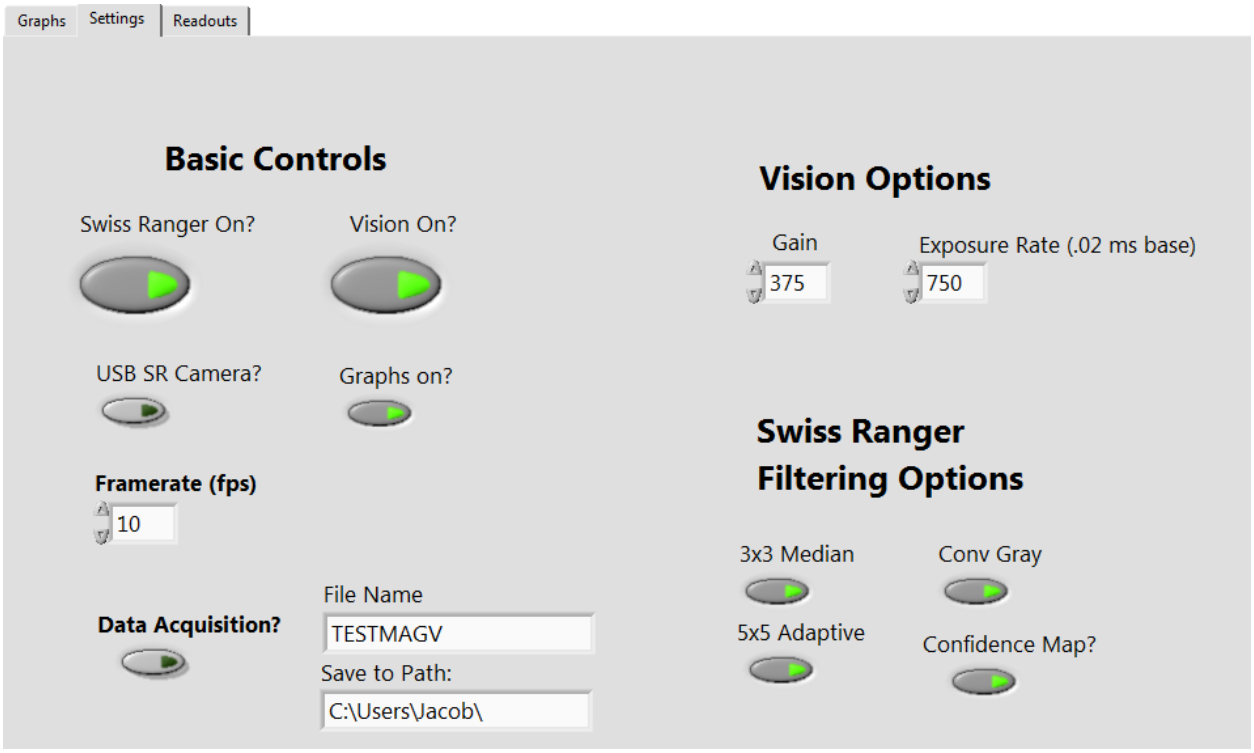

Figure 17. Settings Tab of the Vision/Flash LiDAR VI

Visual images can be stored as either a series of images or as an AVI, their filenames reflect the user defined filename as well as a LabVIEW generated timestamp reflecting the time of frame acquisition. The data collected by the SwissRanger is stored in two tab delimited text files: one storing the amplitude and distance data, and one storing the timestamps. Using Matlab, these files can be imported and processed to produce distance plots in a variety of formats. Two of these images can be seen below in Figure 28. By correlating the point cloud data with the visual spectrum images containing the same timestamps, the combined sensor should be able to parse color as well as directly obtained distance data. This data fusion will produce a sensor similar to stereo-vision sensors without a need to rely on feature point detection and parallax calculations.

Figure 28. Matlab processed distance data. The left image is a Z-Distance plot in which each pixel is color coded based on the Z-Distance from the sensor. The image on the right is a three-dimensional Cartesian point cloud representation of the same frame.

Although Mesa contacted the team, stating that half of the pixel array was incorrectly calibrated, some testing was done to check on the accuracy and repeatability of the sensor. Mesa states on the SR4000 data sheet, that the sensor was tested at 2m against a surface with 99% reflectivity. Under these conditions, the SR4000 has a stated accuracy of ±15mm and a repeatability of 7.2mm (1σ) with a maximum of 10.8mm occurring at any given pixel. To replicate these conditions closely, a flat, off white surface was placed 6 ft (1.83m) from the camera and a line (34 pixels) of data was analyzed across the face. The claims made about the accuracy were confirmed (±11mm measured vs. ±15mm expected), however the claims made about repeatability fell a little short (10.9mm measured, 7.2mm expected). These results are summarized in Table 12.

Given that the sensor may have calibration issues, and the imperfect replication of the stated test conditions, a 1cm accuracy and repeatability from a sensor relying on time of flight data from infra-red LEDs is quite impressive and certainly passable for the project's intended uses. The SwissRanger will eventually be sent in for recalibration and a second round of accuracy and repeatability measurements will be performed upon its return.

Table 12. Summary of accuracy and repeatability testing done on the SwissRanger. The asterisk denotes that although the 19.5mm measurement is high, it was the only pixel with a repeatability this poor.

	Accuracy	Repeatability (1 sigma)	
		Typical	Max
Expected	±15 mm	7.2 mm	10.8 mm
Measured	±11 mm	10.9 mm	19.5 mm *

Cost Analysis. After completing the platform mechanical design, price quotes were requested for the different components and materials needed to build the platform. The cost of the platform design consists of material and mechanical components. The amount of material needed was estimated from preliminary mechanical design. Selection of motors and their cost were based on their power and torque capabilities. These are calculated from friction estimates and speed and battery life goals. As shown in Table 10, the estimated total for the mechanical components and materials of the platform was $5895.97.

Table 12. Mechanical platform parts and materials total cost.

Item	Part Number	Cost (ea)	Quantity	Totals
1x2 6061 Box Tube 1/8" Wall 6' Long	6546K393	$32.05	3	$96.15
2.25x4 6061 Channel 0.19" Base 0.29" Leg 5' Long	1630T18	$55.38	1	$55.38
2x2 6061 Angle 1/8" Thick 8' Long	8982K25	$32.27	1	$32.27
24x24 6061 Sheet 1/8" Thick	89015K48	$71.56	2	$143.12
Lithium Iron Phosphate Battery	Customized	$2232.00	1	$2232.00
Protection Circuit Board	PCM-LFP25.6V100A	$225.95	1	$225.95
Maxon Motor	EC 45 136210	$673.30	2	$1346.60
Gear Head	GP62 110502	$603.70	2	$1207.40
Shunt Regulator	235811	$278.55	2	$557.10
			Total	**$5895.97**

Once research and selection evaluation were completed for all the sensors required for the navigation system and other features, price quotas were requested and all items have been ordered. Sensors such as the Tau 320 IR camera, Scout Machine Camera, Velodyne, IBEO, Swiss Ranger, and Novatel had the largest impact in our budget with a total of $88,066.09. Other expenses include cables, controllers, and modules that are required for sensor and software interface. As shown in Table 13, the total amount spent on sensors and required accessories was $92,567.98.

Table 13. Sensors and required accessories total cost.

Item	Part Number	Cost(ea)	Quantity	Totals
485 Cable		$50	1	$50
Communication Protocol		$180	1	$180
FLIR Tau 320, 9mm	413 20009H-FPNLX	$6500	1	$6500
VPC-Module	421-0039-00	$150	1	$150
Scout Machine Camera SCA640	780884-01	$818.09	1	$818.09
Power Supply for Scout Camera	779986-01	$71.89	1	$71.89
Velodyne	HDL-32E	$29900	1	$29900
IBEO		$18753	1	$18753
Swiss Ranger	R339-SR4000-10M	$9095	1	$9095
Novatel GNS+INS with Antenna	SPAN-CPT	$23000	1	$23000
Roboteq Motor Controller with Encoder	BL1500 BP	$330	2	$660
US Digital E6 Encoders	E6	$95	2	$190
IEC Slip Ring		$3200	1	$3200
			Total	**$92567.98**

Finally, the construction of the 3D sensor mount platform needed to support the 3D Lidar sensor and the Scout camera required ordering various items from different markets. Parts were

ordered from Robot Marketplace, Rose Bopla, Newark, US Digital, EPC, Misumi, and McMaster. The mounting box and rotation mechanism parts and costs are shown in Table 14. The total cost for the 3D sensor mount platform is $4,622.58.

Table 14. 3D Sensor Mounting Box

Item	Part Number	Cost(ea)	Quantity	Totals
Bearing Assembly	8700K100	$204.13	1	$204.13
1-3/8”x12” plastic tube (PETG)	9245K43	$3.84	1	$3.84
1-3/16” hole saw	4066A22	$4.24	1	$4.24
1-1/16” hole saw	4066A19	$4.24	1	$4.24
8-32x1.75 socket screw	90128A206	$0.49	10	$4.89
8-32 threaded spacer	93620A455	$1.39	10	$13.90
Motor mount gusset	RACW40-40-10	$15.20	2	$30.40
Small pulley for motor	TTPA20-AT5100-B-P6	$20.99	1	$20.99
440mm timing belt	TTBU440T5-100	$7.60	1	$7.60
Large pulley with bored hub	TTPA60-AT5100-B-F30-Z35-J10.0-BC3.0	$66.80	1	$66.80
Encoder	775-B-S-4096-R-PU-V-9D-N-N-N	$428.15	1	$428.15
Encoder Reader	QSB-S	$54.84	1	$54.84
3 Pin power connector	BULGIN-PX0730/S	$11.88	1	$11.88
3 Pin power plug, sealed	BULGIN-PX0731/P	$11.88	1	$11.88
USB connector	SAMTEC-SCRU-02	$8.67	3	$26.01
USB plug	SAMTEC-SCPU-17-G-2.00-BMS-AM	$20.11	3	$60.33
RJ 45 connector, sealed	SAMTEC-SCRE-01	$17.63	1	$17.63
RJ 45 plug, sealed both ends	SAMTEC-SCPE-G-02.00-D	$32.84	1	$32.84
Base Enclosure	12340230	$344.01	1	$344.01
Motor	BH31	$23.99	1	$23.99
Motor Controller	Jrk 21v3	$49.99	1	$49.99
			Total	**$4,622.58**

In summary, the majority of the parts and items needed to complete the final design of the vehicle have been ordered and received. The budget for the production of this project is $150,000. Currently, the total cost for the development of the autonomous ground vehicle is $103,089.53.

Ethical Considerations

This autonomous vehicle was being designed as a research platform meant for use over the next few years. It will likely be modified several times throughout its lifetime and will require maintenance from time to time. For these reasons, it is vital that this robot be easily modifiable and operable without danger to the researchers. As with any device which contains electronics, additional consideration must also be taken towards the life cycle and environmental impact of the power system. This project was also being funded by a military grant and thus with tax payer money which demands no misappropriation of funds.

Because the robot must operate at relatively high powers, the drivetrain battery pack is capable of delivering significant currents and could be hazardous if handled incorrectly. The design team had to take care to fully understand the tools necessary to maintain and charge the battery as well as what types of misuse could lead to permanent battery damage. LiFePO4 batteries, like the one specified by the design, are safer than other lithium batteries because they are inherently more stable and less susceptible to explosive thermal runaway [5]. Even so, along with the design a description of proper charging and maintenance protocols are necessary to ensure the batteries are not overloaded. During operation, circuitry is in place to ensure the allowable current draw is not exceeded. Shunt circuitry is also in place to discharge the current produced during braking.

Power is not the only potential danger associated with the robot. The autonomous vehicle has a projected weight of 60kg and will be capable of moving at ten miles per hour. Although the intent of the design is to have a fully autonomous vehicle which would avoid contact with obstacles, it would be irresponsible to implement a final design without both on-vehicle and remote emergency stops in the event of a runaway platform. During testing, the design team has take care to rigorously test the safety measures.

Several components will require eventual replacement, so environmental impact of the design must be considered. The battery, for instance, has a finite cycle life and may be replaced at least once during the robot's life. The battery type selected is non-toxic and easier to recycle than traditional lithium cells while maintaining a high cycle life. Because the frame is being manufactured from scratch, the raw materials will be purchased from suppliers with as little excess as possible to reduce waste.

Financial decisions for this project are particularly important because the funding is supplied through a military grant. The design made every effort to be fiscally responsible, while ensuring the final product meets the high standards of the Army. The allocation of taxpayer

money demands that all design decisions and purchases are immediately pertinent to the development of the proposed research platform.

Performance Testing

After the functional mobile platform was demonstrated, sensing and autonomy capabilities were integrated into the MAGV platform. Using information provided by the INS, waypoint navigation was demonstrated in a large open space with no obstacles present. The vehicle was also able to avoid 'virtual' obstacles entered into the control program. The INS was also used to verify that the maximum speed of the vehicle was in excess of 10 mph.

The MAGV was then taken to compete in the IGVC competition at Oakland University in Rochester, Michigan in June of 2011. The competition involved autonomous path following, obstacle avoidance, and waypoint navigation on a mild off-road terrain consisting of smooth and rutted grassy fields. This proving ground gave us valuable insight to the performance of our design, and allowed us to evaluate several of our previous design decisions, and incorporate our findings in to the construction of a next-generation platform.

In particular, it was found that on soft grass and ground, the vehicle had difficulty accelerating or turning in place after coming to a full stop. The caster wheels that allow the differential steering capability would become stuck, and the power of the drive motors was occasionally insufficient to overcome the initial resistance to get the vehicle moving. Secondly, the lack of a ride suspension on the vehicle caused excessive vibration that eventually lead to a minor structural failure due to material fatigue, despite the fact that the vehicle was driven only on grass and dirt. The limited damping provided by the pneumatic tires of the MAGV was not adequate for high-speed off road operation.

Design Evolution

After the IGVC, a second generation design incorporating our findings was created and called the Mark II. The MkII incorporated independent trailing swingarm suspension for both the drive wheels and the front casters, and drive motors with an increased power rating. Ride height was maintained using coilover spring-damper struts. A CAD mockup of the MkII design can be seen below in Figure 29. The MkII was prototyped prior to formal fabrication, and it was found that the suspension design was unstable and not feasible.

The MkIII was then designed with a high strength independent parallel link suspension in the rear, and an air-spring trailing arm configuration in the front. The diameter of the drive wheels and the under-chassis ground clearance was inreased to improve off road performance, and the overall wheelbase was narrowed to improve manuvering ability in close quarters. A CAD mockup of the MkIII design can be seen below in Figure 30. The viability of the MkIII design was verified by constructing a single platoform before fabrication of the remaining three

vehicles in the fleet was started. The initial MkIII platform, with drive unit assembled but otherwise bare (as seen in CAD renderings) is included in Figure 31, and the platform equipped with drive contols to enable untethered operation, can be seen below in Figure 32.

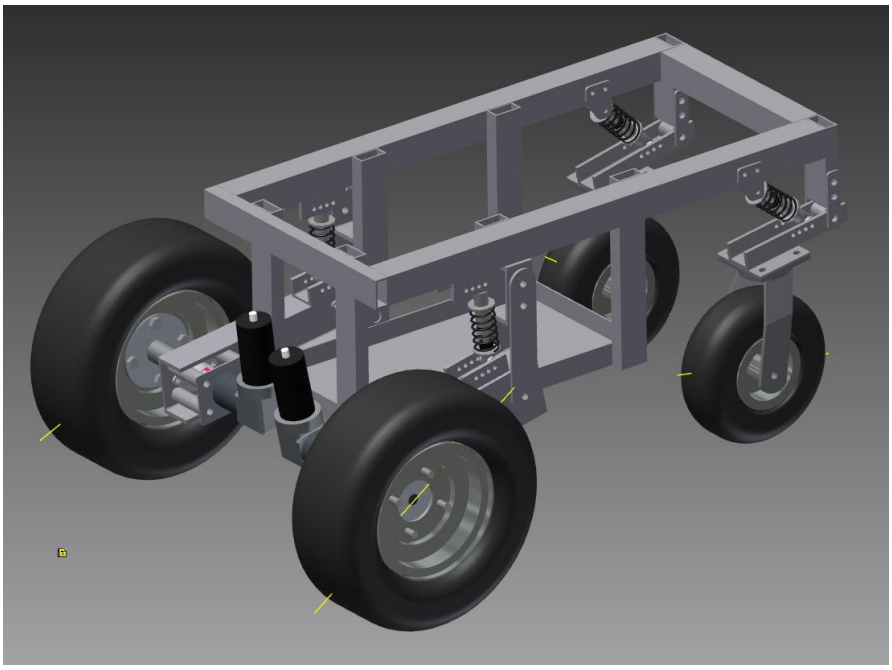

Figure 29. CAD mockup of the MkII design, not constructed due to sub-optimal rear suspension geometry

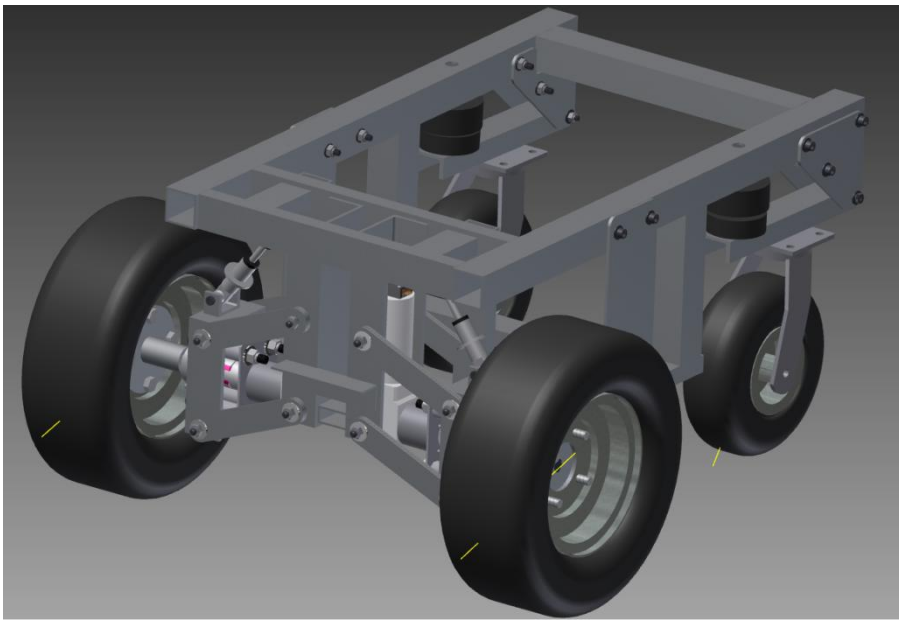

Figure 30. CAD mockup of the MkIII design, detailing rear parallel link suspension and front air-spring swingarms

Figure 31. Bare assembled MkIII, Number 1, ready for installation of power and control electronics

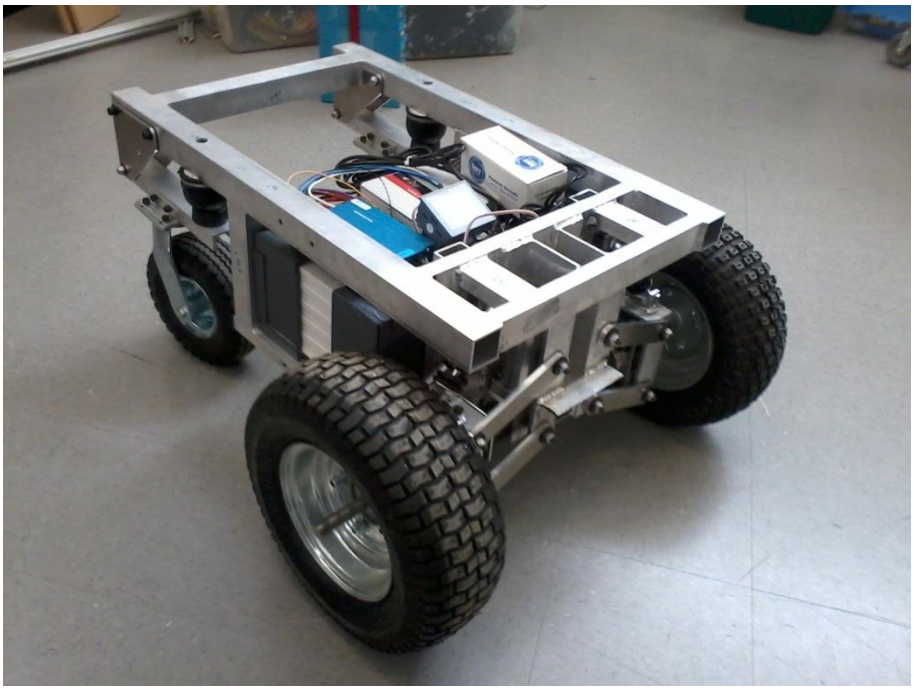

Figure 32. MkIII platform equipped with battery, battery management, and motor control electronics, capable of untethered remote operation

Summary and Conclusions

The MAGV team has used rigorous engineering design techniques to successfully construct, test, and evolve a highly capable autonomous platform well suited to our project requirements. Using the same methods, the team has also equipped the vehicle with an advanced sensing and computational suite that is highly suited to both autonomous navigation and high-bandwidth data collection and compression. The fleet has been demonstrated to be robust and rugged, and is expected to perform exceptionally for many years to come.

References

1. "Clearpath Robotics - Husky." *Clearpath Robotics - Home*. Web. 17 Oct. 2010. <http://www.clearpathrobotics.com/husky.html>.

2. "ARCHER PLATFORMS." *Reflexxrobotics.com*. Web. 17 Oct. 2010. <http://reflexxrobotics.com/products/platforms/archer>.

3. "BOUNDER Plus H-frame." *BOUNDER Power Wheelchairs from 21st Century Scientific, Inc*. Web. 17 Oct. 2010. <http://www.wheelchairs.com/hframe_plus_page.html>.

4. 21st Century Scientific. "21st CentruyRetialQoutation." Letter to Matt Pyrak. 13 Oct. 2010. MS.

Appendices

Appendix A: Customer Needs and House of Quality

Appendix B: Project Plan and Gantt Chart

Appendix A: Customer Needs and House of Quality

House of Quality: *UGV Research Platform Team*

Date: 10/15/2010

Author: **Team Name:** UGV Research Platform Team
CRN: 94249
Members Names: Jacob Lambeth
Kyle Laaker
Matt Pyrak
Fulton Smith
Adam Deng
Yami Hernandez
Braden O'Meara
Tim Battis

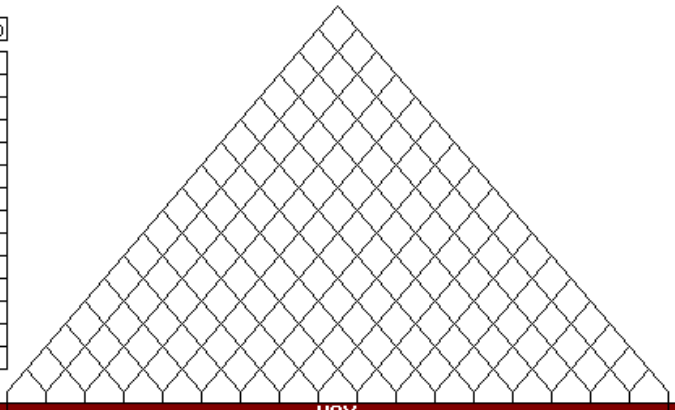

VHO					HOV																NOV				
Army	IGVC	Researchers			Maximum clearqble curb/pothole	Maximum incline	Time until recharge	Turning radius	maximum payload	Number of ports available	Maximum speed	Max temperature	Min temperature	Rate of percipitation can handle	Noise level	Obstacle detection range	E-stop available	Positional accuracy	Data storage space	Processor speed	People liking design	1	2	3	4	5
				Direction of Improvement	▲	▲	▲	▼	▲	▲	▲	▲	▼	▲	▲	▲	▲	▲	▲	▲	▲					
				Units	in	deg	hr	ft	lbs	#	mph	°F	°F	in/hr	dB	ft	y/n	ft	Gb	GHz	%					
10	7	7	VHAT	Performance: Travel on rugged terrain	●	○					○			○												
9	3	8		Performance: Long battery life		○	●		○		○									○						
6	3	8		Performance: Good turning radius				●																		
8	5	7		Performance: Carry large payload			○		●		○															
6	1	10		Performance: Easily modifiable					○	●																
7	2	8		Performance: Moves at reasonable speed			○		○		●															
9	4	7		Environment: Withstand broad temperature range								●	●	○												
8	5	6		Environment: No effects from rain										●												
5	6	9		Environment: No effect from EM interference											●											
				Environment:																						
				Environment:																						
5	10	9		Autonomy: Can avoid obstacles				○								●		○								
4	10	5		Autonomy: Has emergency shutdown													●									
7	10	9		Autonomy: Can travel to waypoints												○		●								
6	7	8		Autonomy: Can store data locally															●	●						
				Autonomy:																						
9	8	4		Aesthetics: Professional look																	●					
				Aesthetics:																						
				Aesthetics:																						
				Aesthetics:																						
				Aesthetics:																						
				Archer E																						
				Bounder Plus																						
				Husky																						
				Target (delighted)																						
				Target (disgusted)																						

Figure A.1. Based on the customer needs and engineering performance measures, the above house of quality was developed to assist in the product design processs